

A Study of the Stretch-Induced Softening Behavior
Of Particle Filled Elastomers

By

Andrea Greb

Submitted to the Department of Mechanical
Engineering in Partial
Fulfillment of the Requirements for the
Degree of

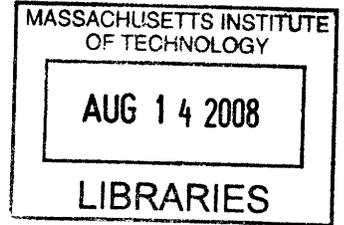
Bachelor of Science

at the

Massachusetts Institute of Technology

June 2008

© June 2008 Andrea Greb
All rights reserved



The author hereby grants to MIT permission to reproduce and to
distribute publicly paper and electronic copies of this thesis document in whole or in part
in any medium now known or hereafter created.

Signature of Author.....

Department of Mechanical Engineering
May 9, 2008

Certified by

Mary C. Boyce
Professor of Mechanical Engineering
Thesis Supervisor

Accepted by

John Lienhard
Chairman, Undergraduate Thesis Committee

A Study of the Stretch-Induced Softening Behavior
Of Particle Filled Elastomers

By
Andrea Greb

Submitted to the Department of Mechanical Engineering
on May 9, 2008 in partial fulfillment of the
requirements for the Degree of Bachelor of Science
in Mechanical Engineering

ABSTRACT

Elastomers are able to undergo relatively large deformations in an elastic manner, which makes them the material of choice for a wide range of applications. In some cases, filler particles, such as carbon black, are added to the elastomer to alter the mechanical behavior when subjected to different loading conditions. When subjected to cyclic loading conditions, elastomers undergo stress-induced softening, known as the Mullins effect, and this softening behavior is influenced by the amount of filler particle present. The softening is considered to be an evolution of the soft and hard domain microstructure of the material, with the effective soft domain increasing with stretch. In this study, finite element analysis will be used to understand the softening behavior of particle reinforced elastomers. The softening behavior of the parent elastomer will be modeled using a constitutive model proposed by Qi and Boyce (2004). Nonlinear finite element analysis using the ABAQUS code was used to model elastomers with various volume fractions of filler particles, and the stress-strain behavior of the composite and evolution of the soft domain within the matrix is computed. The addition of filler particles was found to increase the overall stiffness of the elastomer, but also to increase the stretch-induced softening, and to alter the distribution of soft domains within the material. The presence of occluded regions of matrix material was also found to have a significant effect on softening behavior.

Thesis Supervisor: Mary C. Boyce

Title: Professor of Mechanical Engineering

Table of Contents

| | |
|--|----|
| 1 Introduction..... | 4 |
| 1.1 Background..... | 4 |
| 1.2 Previous Research..... | 5 |
| 2 Model..... | 7 |
| 2.1 Explanation of Model..... | 7 |
| 2.2 MATLAB modeling of model..... | 8 |
| 2.3 Testing use of model in ABAQUS..... | 12 |
| 2.4 Application of model to experimental data..... | 13 |
| 2.4.1 Determination of material parameters for unfilled rubber..... | 13 |
| 2.4.2 Micromechanical modeling of filled rubber..... | 16 |
| 3 Results..... | 19 |
| 3.1 Effect of particle volume fraction on stress-strain behavior when matrix does not soften..... | 19 |
| 3.2 Effect of particle volume fraction on stress-strain behavior when matrix undergoes stretch-induced softening | 26 |
| 3.3 Effects of occluded region on matrix..... | 50 |
| 4 Conclusion..... | 60 |
| References..... | 61 |

1 Introduction

1.1 Background

Elastomers are able to undergo relatively large deformations in an elastic manner, which makes them the material of choice for a wide range of applications. In some cases, filler particles, such as carbon black, are added to the elastomer to alter the mechanical behavior when subjected to different loading conditions. The addition of filler particles alters behavior in three ways: increasing the stiffness of the rubber, altering the strain history dependence of the stiffness, and altering time dependent aspects of the material including hysteresis and stress relaxation. [3]

One behavior affected by the addition of filler particles is stretch-induced softening. Elastomeric materials undergo stress or stretch-induced softening, known as the Mullins effect, when subjected to cyclic loading conditions. Upon repeated loading, the material will exhibit more compliant behavior than it did when originally loaded. This softening behavior is increased when filler particles are added, as shown in Figure 1.1. [8]

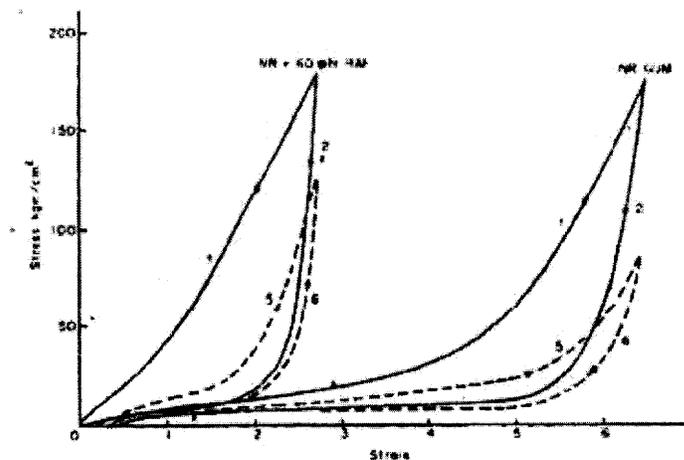


Figure 1.1 Cyclic uniaxial tension stress strain results from Harwood and Payne (1966): The curve on the right is for an unfilled rubber, the curve on the left is for a filled rubber. Softening is more significant in the filled rubber at much lower strains than it does for the unfilled rubber. [8]

There are two main theories as to why the addition of filler particles causes greater softening. One theory considers the increased stiffness that results from the addition of stiff filler particles to be a result of attachments between the rubber and filler particles providing additional restrictions on the cross-linked network. Increased softening occurs when these attachments are loosened or broken. [5]

The second theory considers softening to be an evolution of soft and hard domains within the elastomer. Stretching of the elastomer produces a quasi-irreversible rearrangement of the molecular networks, resulting in a rearrangement of hard and soft domains, which effectively increases the volume fraction of the soft domain. [5]

1.2 Previous Research

Elastomers consist of a network of long chain macromolecules, which are either cross linked covalently, physically entangled, or both. The deformation behavior of rubber can be modeled as the stretching of a network of these chains. These chains have N rigid links of equal length l , with a limiting extensibility of the final length divided by the initial length, given as $\lambda_L = \sqrt{N}$, and the chain length is considered the distance between cross-links. [1]

The theory of softening which will be examined in this thesis was initially posed by Mullins and coworkers. [9] This theory considers softening to be an evolution of soft and hard domains within the rubber. Stretch produces a rearrangement of the soft and hard domain regions of the molecular network, which occurs when molecular chains are stretched, either exposing occluded soft domains or breaking apart hard domains. This deformation and rearrangement displaces network junctions from their original location, and thus produces a rearrangement of hard and soft domains in the material and

effectively increases the volume fraction of soft domain. The volume of soft domain is denoted by v_s . Evolution of v_s occurs when previously occluded regions of soft domain are released with deformation. It is assumed that once these domains are released, they will remain soft; that is, the softening is permanent and v_s remains at the maximum value achieved during deformation even after the material is released. The structural state of the material is characterized by $\Lambda_{\max \text{ chain}}$, which is the maximum local chain stretch in the deformation history. When a material is released from a stretch and then re-stretched, evolution in v_s only begins after the chain stretch reaches a value above the previous $\Lambda_{\max \text{ chain}}$. [2]

In this approach to softening, filled rubbers are treated as a composite system and the concept of amplified strain is used to explain the greater softening observed in filled rubbers compared to unfilled rubbers. In filled rubbers, the average strain of the elastomeric domains is amplified over the macroscopic strain, due to the inclusion of filler particles which do not accommodate much of the macroscopic strain. This amplified stretch can be represented by $\Lambda = 1 + X(\lambda - 1)$ where X is an amplification factor which depends on particle volume fraction and distribution, and λ is the macroscopic axial stretch. It was proposed that cyclic softening is a property of unfilled rubber, and the softening is greater for filled rubbers because of the amplified strain resulting from the inclusion of filler particles. Later work has given more insight into the effect of filler particles. Micromechanical modeling of particle filled rubbers has shown that rubber can be trapped within aggregates of filler particles, thus increasing the effective volume fraction of filler. When the material is stretched, this rubber is released, and contributes to softening. [2]

Another theory of softening states that softening is the result of some form of debonding of the particle/matrix interface. [4] [6] The inclusion of rigid particles is thought to increase stiffness because the particle/matrix attachments increase the amount of restrictions on the cross-linked rubber chains. Subsequent softening of the material occurs from the loosening or breaking of some of these attachments. Others generalized this softening to result from relative motion of the rubber and carbon filler particles, and sometimes local separation of the rubber and filler. [6] [7] [10]

2 Model

2.1 Explanation of model

The first step taken in modeling the softening behavior of elastomers was to implement the constitutive model equation of Qi and Boyce for the softening of elastomeric materials in MATLAB. Following Qi and Boyce (2004) when a material is subjected to uniaxial tension/compression the Cauchy stress σ is given by

$$\sigma = \frac{v_s X \mu}{3 \Lambda_{chain}} \frac{\sqrt{N}}{\Lambda_{chain}} L^{-1} \left(\frac{\Lambda_{chain}}{\sqrt{N}} \right) (\lambda^2 - \lambda^{-1}), \quad (1)$$

where v_s is the volume fraction of soft domain, μ is the initial modulus of the soft domain region, N is the number of rigid links between crosslinks of the soft domain region, and L^{-1} is the inverse Langevin function, for the Langevin function defined as $L(\beta) = \coth \beta - (1/\beta)$.

Additionally, in eqn. (1)

$$X = 1 + 3.5v_f + bv_f^2, \quad (2)$$

where v_f is the volume fraction of the hard domain $v_f = 1 - v_s$, and the amplified chain stretch in the matrix, Λ_{chain} , is given by

$$\Lambda_{chain} = \sqrt{X(\bar{\lambda}^2 - 1) + 1}, \quad (3)$$

where $\bar{\lambda}^2 = I_1 / 3$ and $I_1 = \lambda_1^2 + \lambda_2^2 + \lambda_3^2$, where $\lambda_1, \lambda_2, \lambda_3$, are the principal values of the macroscopic stretch (i.e., the stretch of the composite material).

The dependence of the softening rate \dot{v}_s is given by

$$\dot{v}_s = A(v_{ss} - v_s) \frac{\lambda_{chain}^{lock} - 1}{(\lambda_{chain}^{lock} - \Lambda_{chain}^{max})^2} \dot{\Lambda}_{chain}^{max}, \quad (4)$$

Where $\lambda_{chain}^{lock} = \sqrt{N}$ is the locking stretch of a molecule chain, and

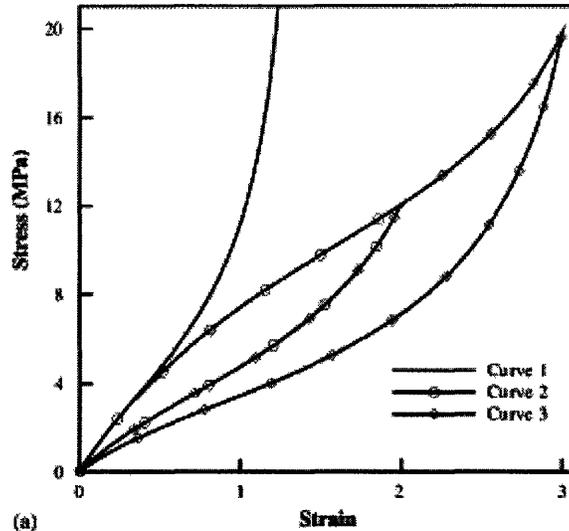
$$\dot{\Lambda}_{chain}^{max} = \begin{cases} 0, & \Lambda_{chain} < \Lambda_{chain}^{max} \\ \dot{\Lambda}_{chain}, & \Lambda_{chain} \geq \Lambda_{chain}^{max} \end{cases}. \quad (5) \quad [11]$$

2.2 MATLAB modeling of model

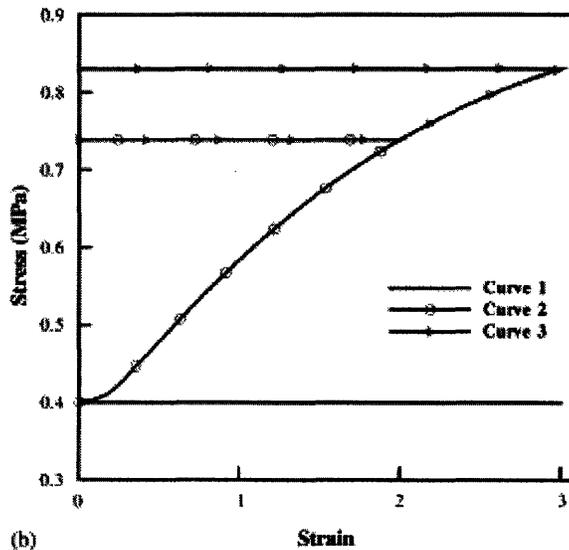
This model was implemented in MATLAB. An iterative scheme was used to find Λ_{chain} , and the inverse Langevin function: was approximated using a Padé approximation

$$L_C^{-1}(x) = x \frac{3 - x^2}{1 - x^2}. \quad (6)$$

Results using the material properties $N=14, \mu=1, A=0.7, v_{s0}=0.4, v_{ss}=0.85$, as obtained by Qi and Boyce are shown in Figure 2.1, and can be compared to the results obtained from implementing the model in MATLAB, shown in Figure 2.2.



(a)



(b)

Figure 2.1 (a) shows the stress strain data given by the Qi and Boyce model for the case of no softening (Curve 1), and with softening: loading to a strain of 2 (Curve 2) and loading to a strain of 3 (Curve 3). Note that when the material is reloaded to a strain of 3, it initially follows the unloading path of Curve 2. (b) shows strain versus softening for for the case of no softening (Curve 1), and with softening: loading to a strain of 2 (Curve 2) and loading to a strain of 3 (Curve 3). When unloaded from a strain of 2, the v_s remains at a constant level, and stays constant during reloading until it is loaded past the previous maximum stretch. [11]

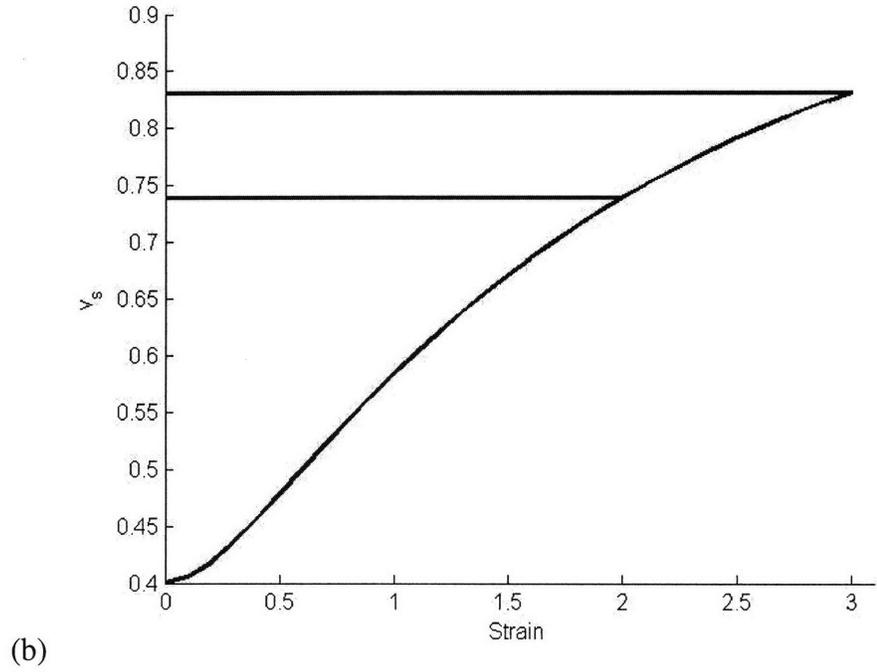
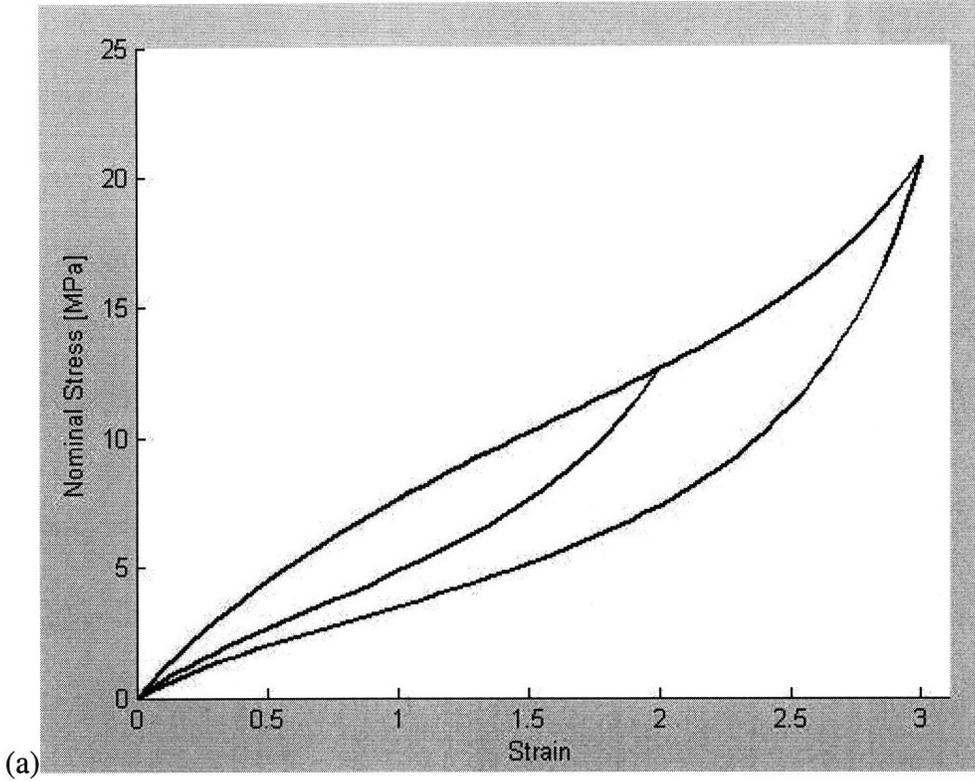


Figure 2.2 shows the Qi and Boyce model as plotted in MATLAB, using an iterative scheme and an approximation for the inverse Langevin function, for strains of 2 and 3. This figure replicates the results presented in Qi and Boyce's paper, showing that the iterative scheme and approximation for the Langevin function gives reasonable results. (a) shows the results for the stress-strain curve, and (b) shows the evolution of v_s .

As seen in Figure 2.1 (a), in the case of no softening, the stress-strain behavior is identical for the loading and unloading cases, as seen in Curve 1. When softening occurs, the material exhibits a more compliant behavior upon unloading, as seen in Curve 2. When reloaded, the material exhibits this same compliant behavior until it is loaded past the initial load, as seen in Curve 3. Upon unloading, the material has softened further, and thus exhibits even more compliant behavior. The evolution of v_s for a given strain is shown in Figure 2.1 (b). For the case of no softening, Curve 1, v_s remains constant. When softening occurs, as in Curve 2 and Curve 3, v_s increases as the material is loaded, and remains constant at the maximum v_s achieved upon unloading. This v_s is maintained upon reloading, until the material is placed under a greater strain than it has already experienced, at which point v_s again begins to increase.

Comparison of the results obtained from the model with experimental data obtained by Mullins and Tobin (1957) shows excellent agreement, as seen in Figure 2.3.

[11]

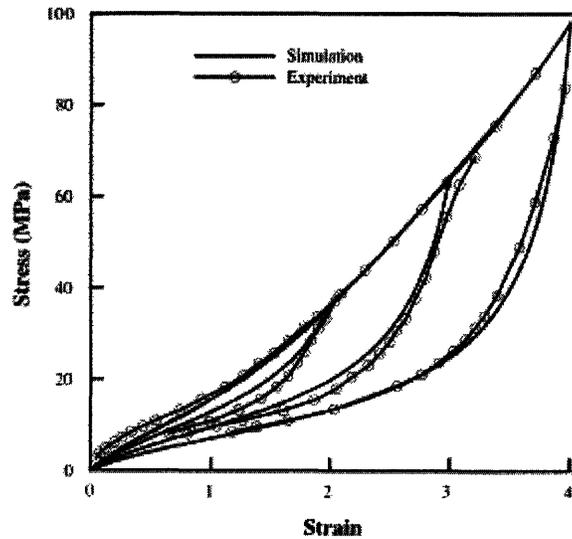


Figure 2.3 shows the comparison between the Mullins and Tobin data and that given by the Qi and Boyce model for strain levels of 2, 3, and 4. [11]

2.3 Testing use of model in ABAQUS

Using ABAQUS, a mesh consisting of a single axisymmetric element was created (this mesh can be seen in Figure 3.1a). The material constitutive behavior was inputted through a UMAT subroutine, which was tested to see if Qi and Boyce's results could be replicated. Force and displacement data were taken from the simulation and used to calculate stress and strain. The value of v_s at each integration point was output for each step of the simulation, and a weighted average was taken to determine v_s at each level of strain. As shown in Figure 2.4, the results of the ABAQUS simulation are identical to those seen in the MATLAB modeling.

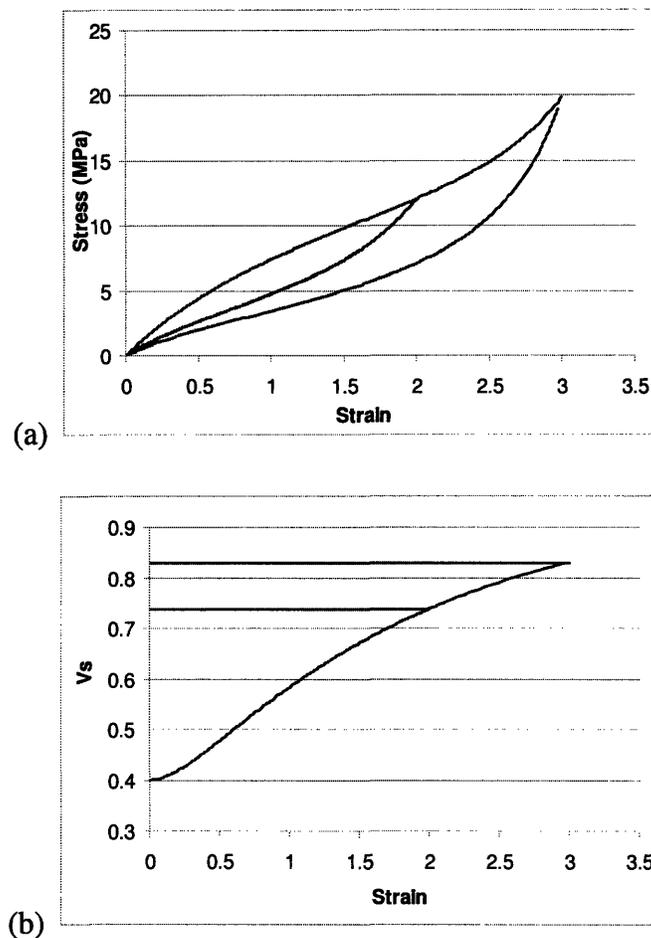


Figure 2.4 shows data for a 6x6 element using softening conditions as given by the Qi and Boyce model; (a) shows a stress strain curve for a loading to a strain of two, followed by unloading and reloading to a strain of 3, and unloading; (b) shows the evolution of the soft volume under the same conditions.

2.4 Application of model to experimental data

2.4.1 Determination of material parameters for unfilled rubber

To validate the model, an attempt was made to replicate experimental results. Through analysis, material properties were determined such that the model captured the behavior of the results of a 1966 study by Harwood and Payne, shown in Figure 2.5. [8]

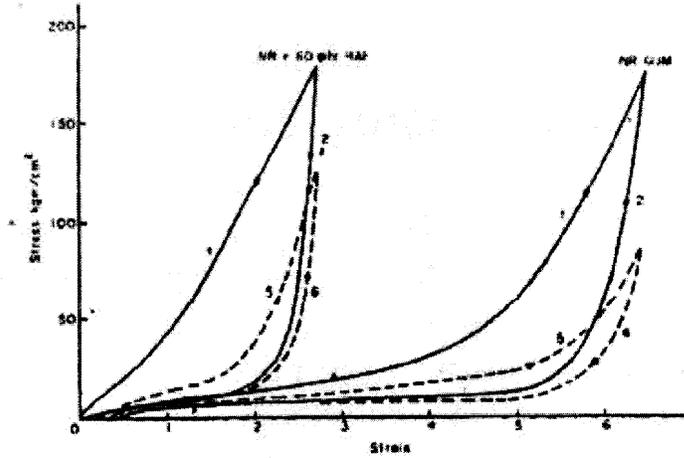


Figure 2.5 shows the stress softening of rubber for an unfilled rubber (the curve on the right) and a filled rubber with 60 PHR, or a 23% volume fraction of filler particles (the curve on the left). [8]

To accomplish this, a graph of the stress-strain behavior for uniaxial tension was

created, using the following equation:
$$f = \frac{v_s X \mu}{3} \frac{\sqrt{N}}{\Lambda_{chain}} L^{-1} \left(\frac{\Lambda_{chain}}{\sqrt{N}} \right) (\lambda - \lambda^{-2}), \quad (7)$$

where f is the nominal stress, and Λ_{chain} is the amplified stretch in the soft domain

$$\Lambda_{chain} = \sqrt{\frac{X}{3} (\lambda^2 + \lambda^{-1} - 3) + 1},$$

λ is the applied axial stretch, and the other variables are as previously defined. [11] This equation simulated the loading and unloading curve of the unfilled rubber, and assumed that the final soft volume fraction would be .95. The material properties were determined

to be $N=20.6$, $\mu=1.2$, $A=0.2$ and the bulk modulus was set equal to 100000, which gave the unloading curve shown in Figure 2.6.

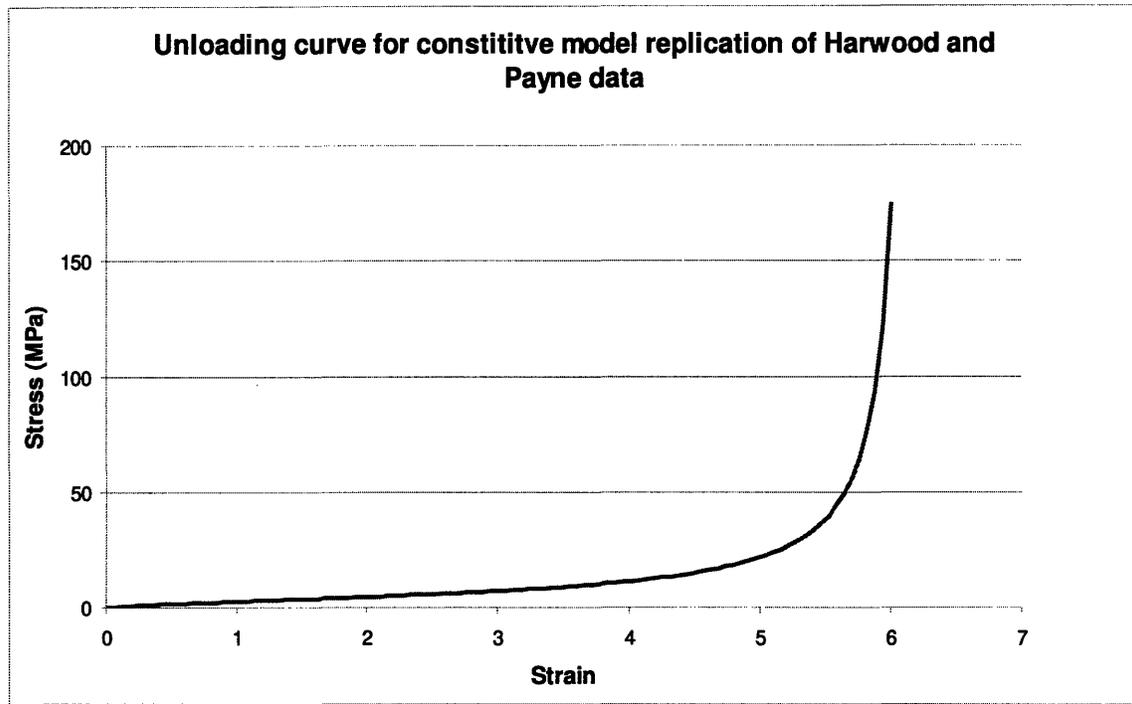


Figure 2.6 shows the stress strain curve for the unloading of a material with properties $N=20.6$, $\mu=1.2$, $A=0.2$ and a final $v_s=.95$.

These material properties were then used in ABAQUS so that the loading curve could be plotted, and the initial soft volume fraction determined. From this data, it was determined that the initial $v_s=.4$. The stress strain behavior and the evolution of the soft domain to a strain of 6 are shown in Figure 2.7 and Figure 2.8. The stress strain curve for repeated loading and unloading is shown in Figure 2.9. The loading curves match with the overall curve when the material is loaded to a strain of 6.

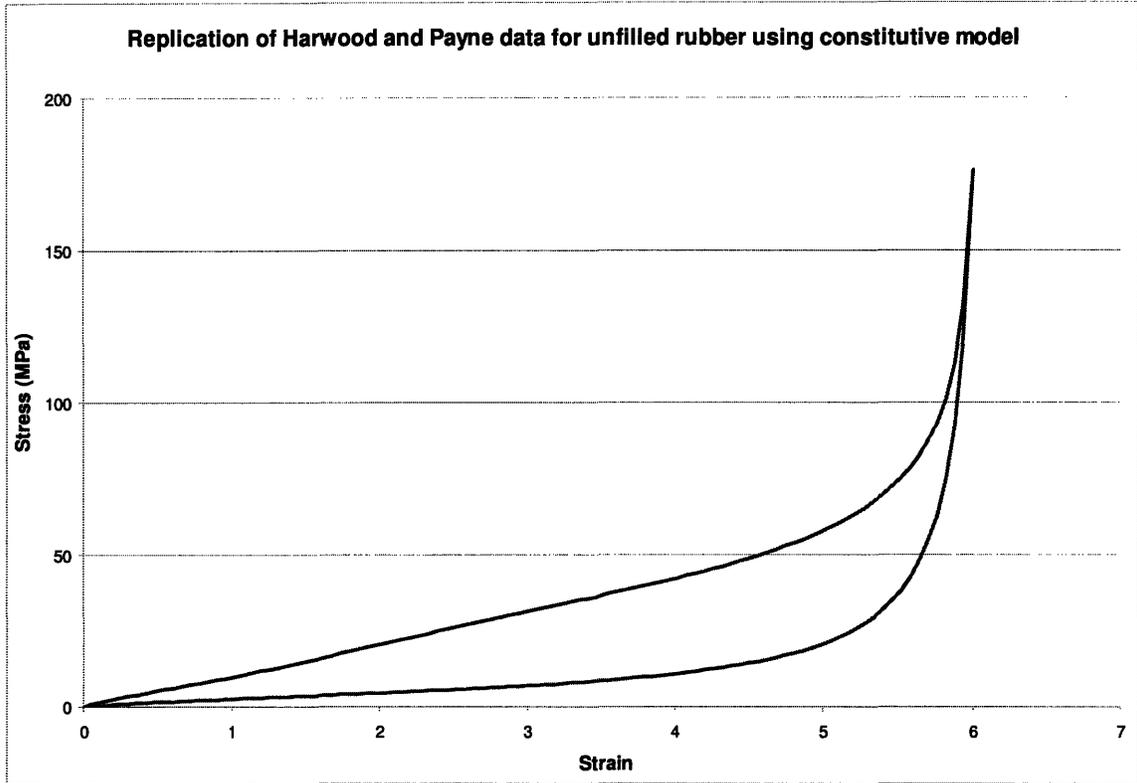


Figure 2.7 shows the loading and unloading behavior of a material with properties $N=20.6$, $\mu=1.2$, $A=0.2$, $v_s=.4$ as modeled in ABAQUS.

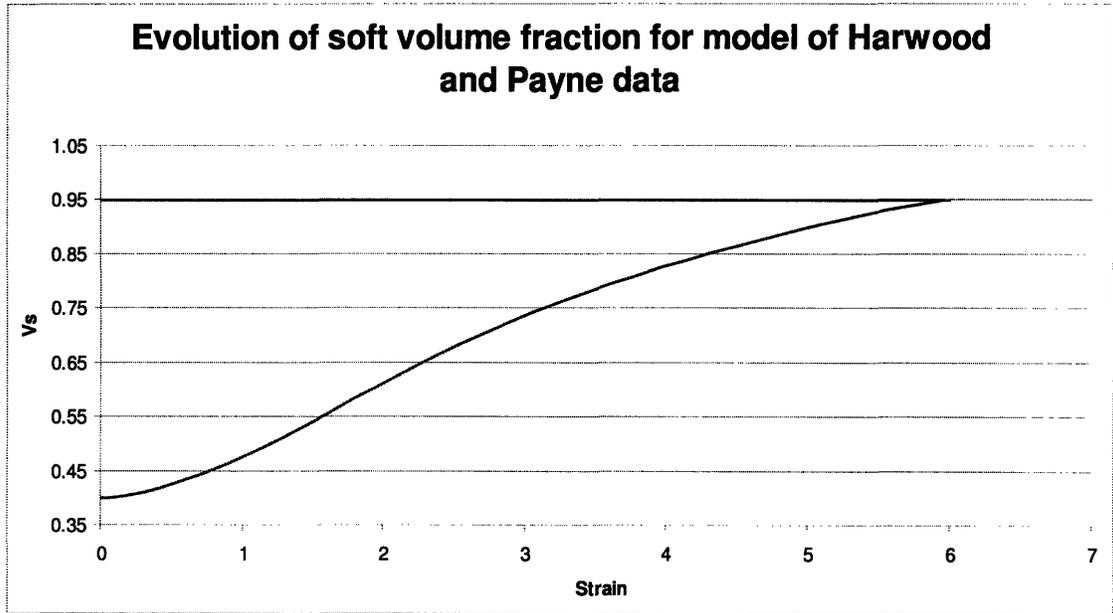


Figure 2.8 shows the evolution of the soft volume fraction behavior of a material with properties $N=20.6$, $\mu=1.2$, $A=0.2$, $v_s=.4$ as modeled in ABAQUS.

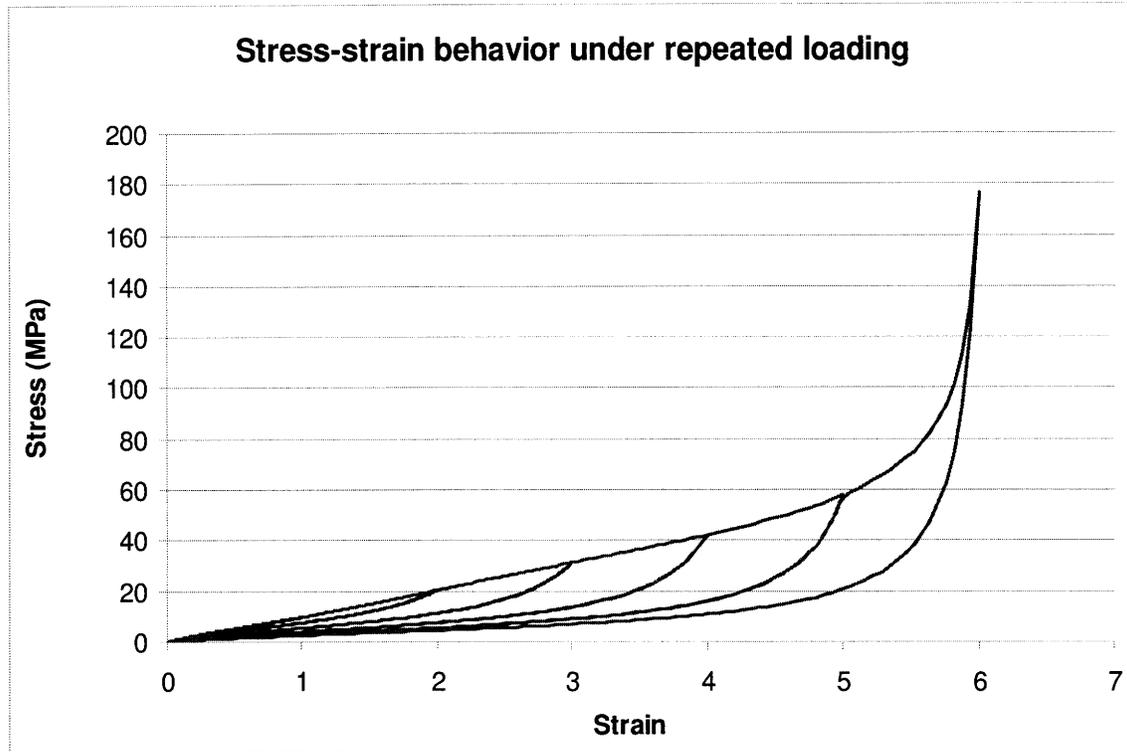


Figure 2.9 shows the loading and unloading behavior of a material with properties $N=20.6$, $\mu=1.2$, $A=0.2$, $\nu_s=4$ as modeled in ABAQUS, at strains of 1,2,3,4,5,and 6.

2.4.2 Micromechanical modeling of the filled rubber

The next step was to take the properties determined for the unfilled rubber, and apply them to a sample with 60 PHR carbon black, or approximately a 23% volume fraction of hard particles. This was done by using axisymmetric elements in ABAQUS with boundary conditions which simulated the inclusion of spherical particles accounting for 23% of the volume fraction. The element was constrained along its left and bottom edges, as well as along a circular edge that simulated the inclusion of a rigid particle. The element also followed boundary conditions given for a cylindrical axisymmetric unit cell representative volume element by Socrate and Boyce (2000): For an element characterized by an initial radius R_0 and initial height H_0 , shown in Figure 2.10 , when

axisymmetric loading about the z -axis is applied to the material, geometric compatibility of deformation in the two families of antisymmetric cells requires that

$$[R(\xi)]^2 + [R(H_0 - \xi)]^2 = 2[R(\xi = 0.5H_0)]^2; \quad (8)$$

where $R(z) = R_0(z) + u_r(z)$ and ξ denotes the axial coordinate for points at the outer radius of the cell in the undeformed configuration. Also, to enforce symmetry of the axial deformation about the cell midplane ($z = H/2$) for the two families of antisymmetric

$$u_z(\xi) + u_z(H_0 - \xi) = 2u_z(\xi = 0.5H_0) : (9). \quad [5]$$

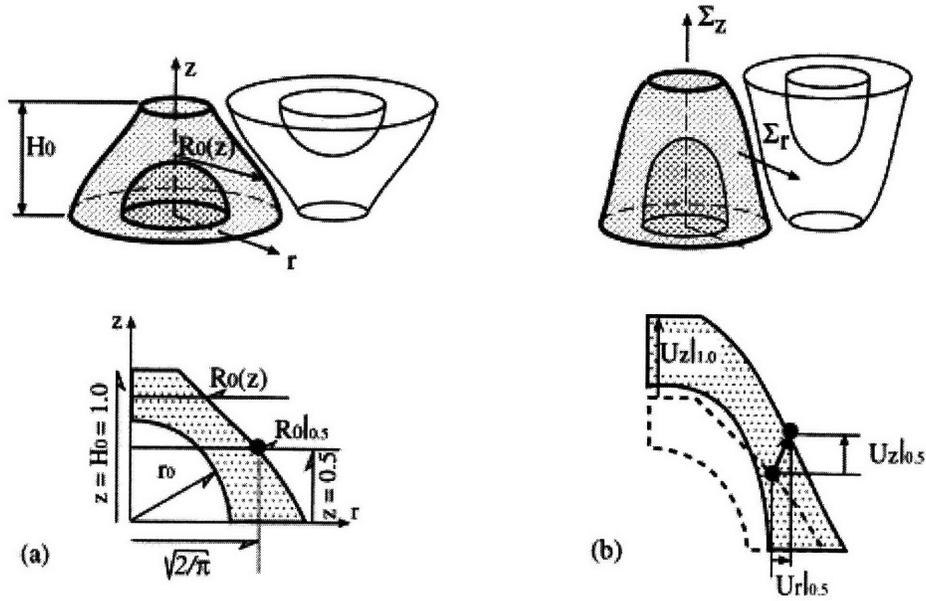


Figure 2.10 shows the representative volume element in undeformed (a) and deformed (b) configurations. [5]

This model and boundary condition type captures the behavior of a staggered array of particles, as shown in Figure 2.11.

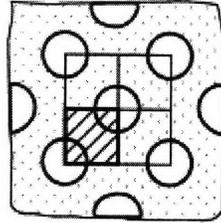


Figure 2.11 shows a staggered square array of particles. The element type used here would look like half of what is shown in the shaded box. [5]

The mesh for this model is shown in Figure 2.12 and was deformed to the maximum strain allowed by the simulation, using the same material properties determined for the virgin rubber.

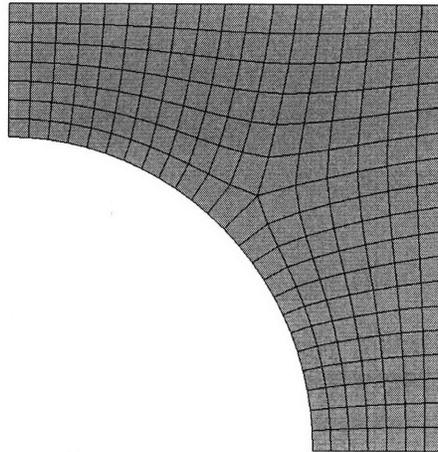


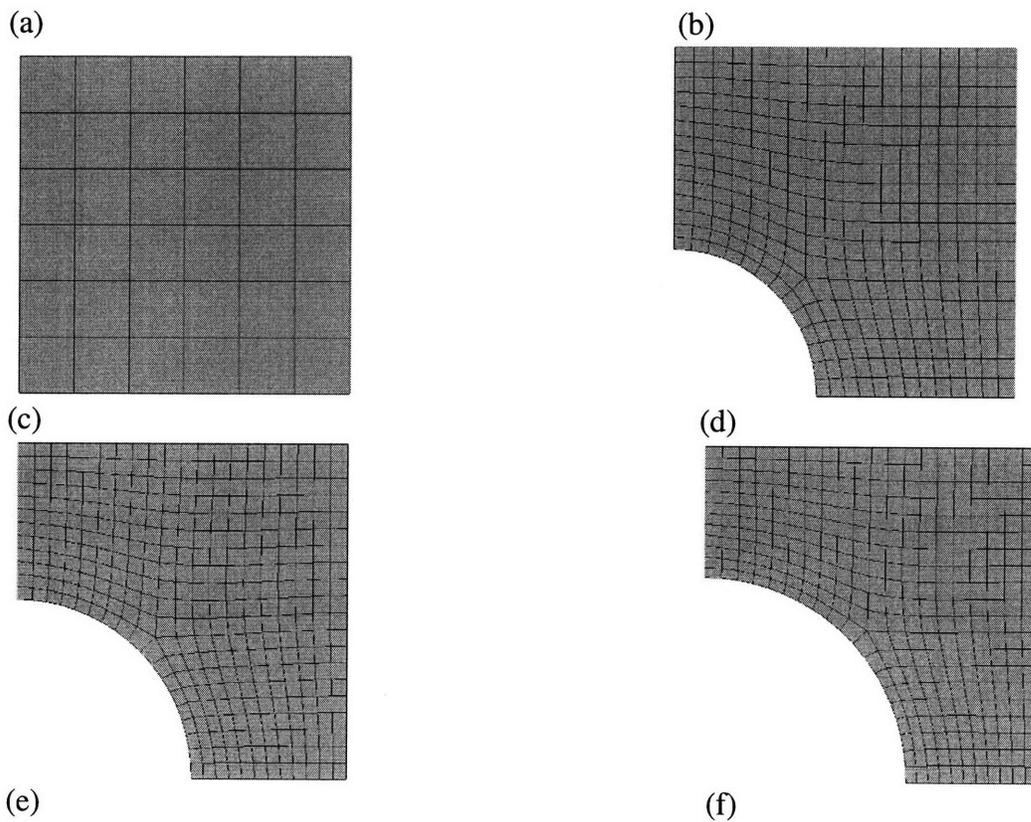
Figure 2.12 shows the undeformed element with a 23% volume fraction.

3 Results

Using the material properties found for the rubber in the Harwood and Payne data, an analysis was done of the deformation behavior of the material for different volume fractions of filler particles: 0%, 5%, 10%, 15%, 20%, 25%, 30%, and 35%. Meshes for these elements are shown in Figure 3.1.

3.1 Effect of particle volume fraction on stress-strain behavior when matrix does not soften

First, the analysis was done without any softening effect (vs is held constant to its initial value).



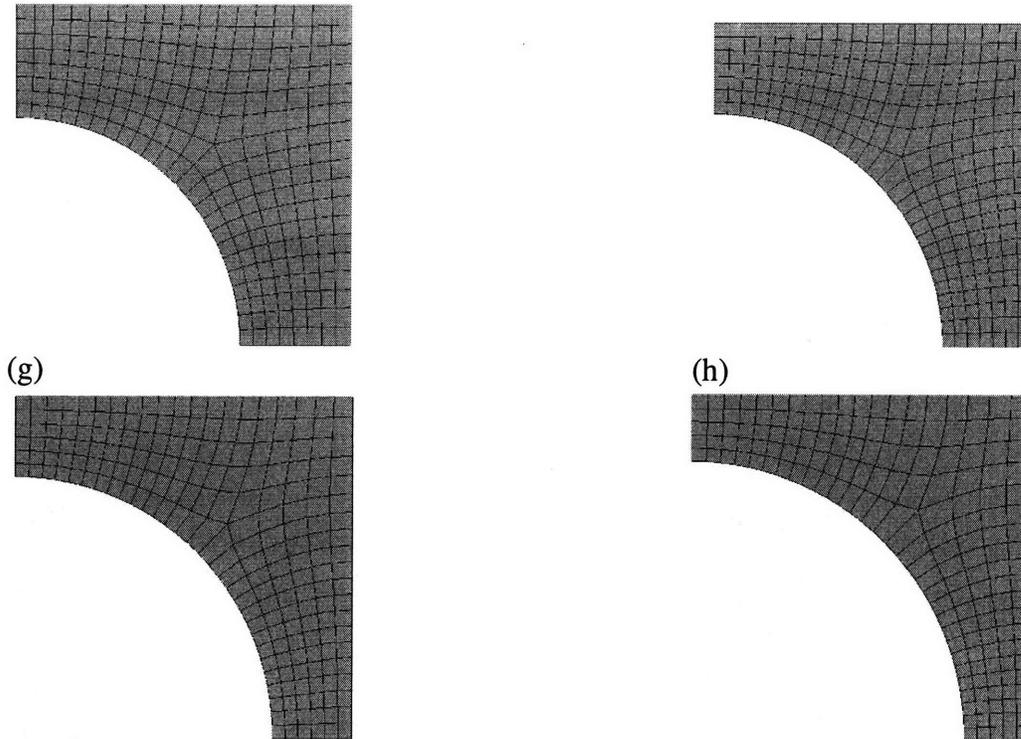


Figure 3.1 shows the initial undeformed meshes for volume fractions (a) 0%, (b) 5%, (c) 10%, (d) 15%, (e) 20%, (f) 25%, (g) 30%, (h) 35%.

The model was stretched along the top edge, to the largest stress allowed by the simulation. The results are shown in Figure 3.2. To better see the difference between unfilled rubber, a small amount of filler, and a large amount of filler, three cases are highlighted in Figure 3.4.

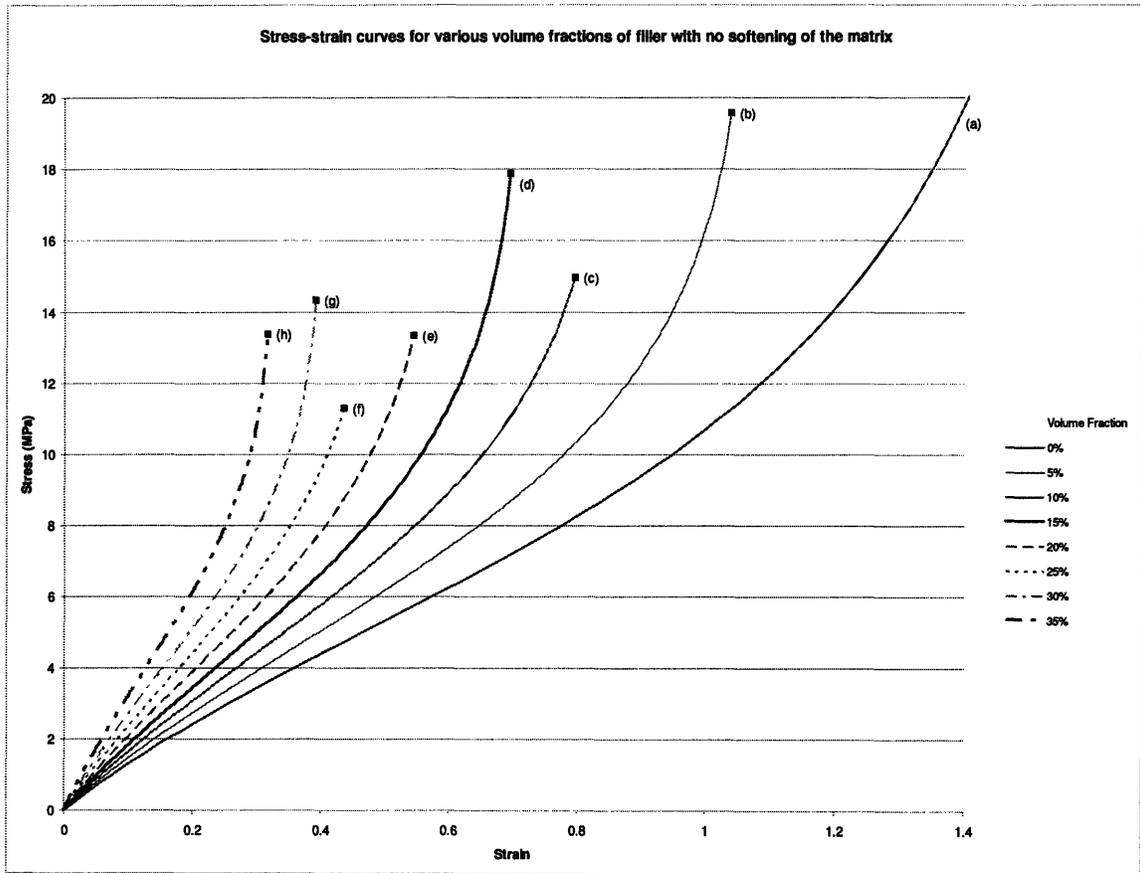


Figure 3.2 shows the stress-strain curves for the loading of rubber which undergoes no softening with increasing volume fractions of filler particle.



Figure 3.3 shows the stress distribution in the 22 direction for each of the positions indicated on the graph; (a) 0%, (b) 5%, (c) 10%, (d) 15%, (e) 20%, (f) 25%, (g) 30%, (h) 35%.

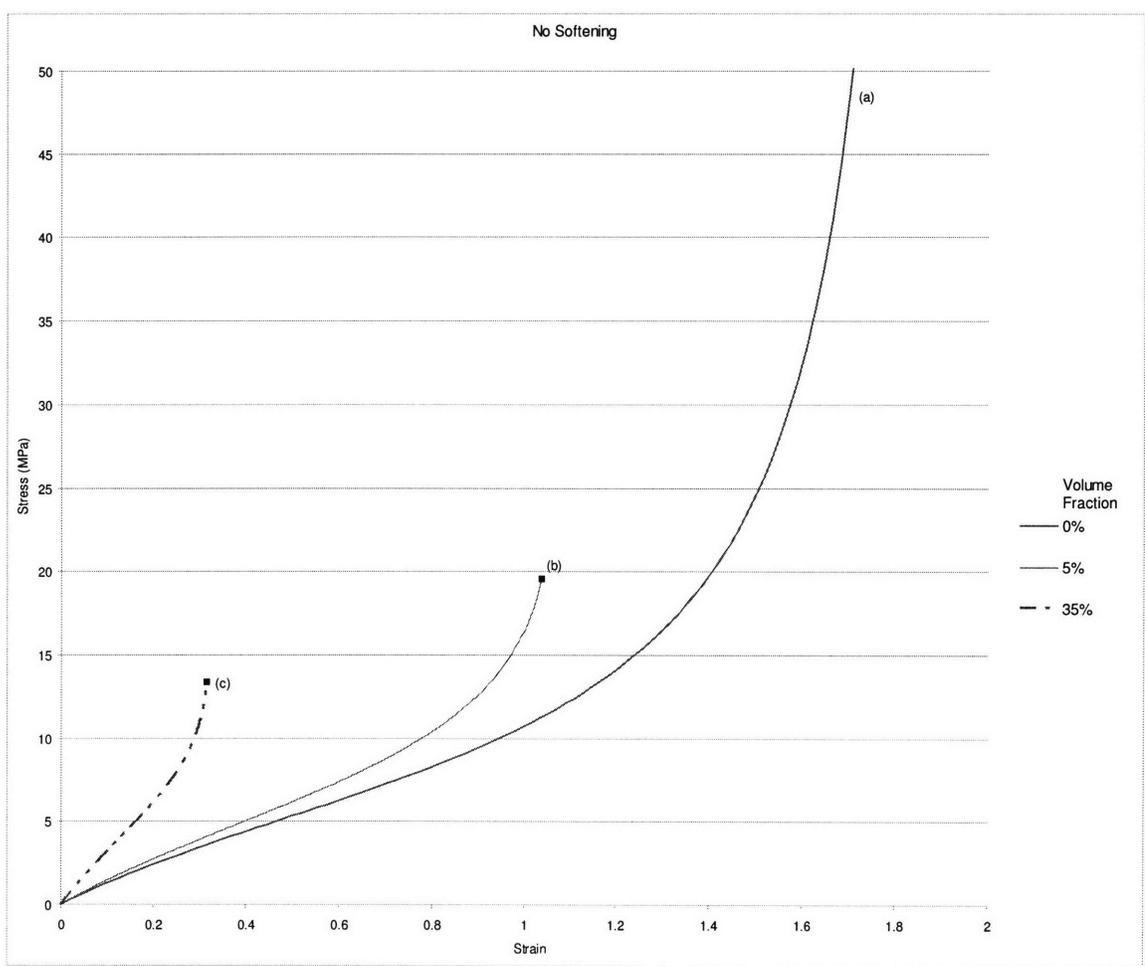


Figure 3.4 shows the stress-strain behavior for material with no filler particles, a 5% volume fraction of filler, and a 35% volume fraction of filler.

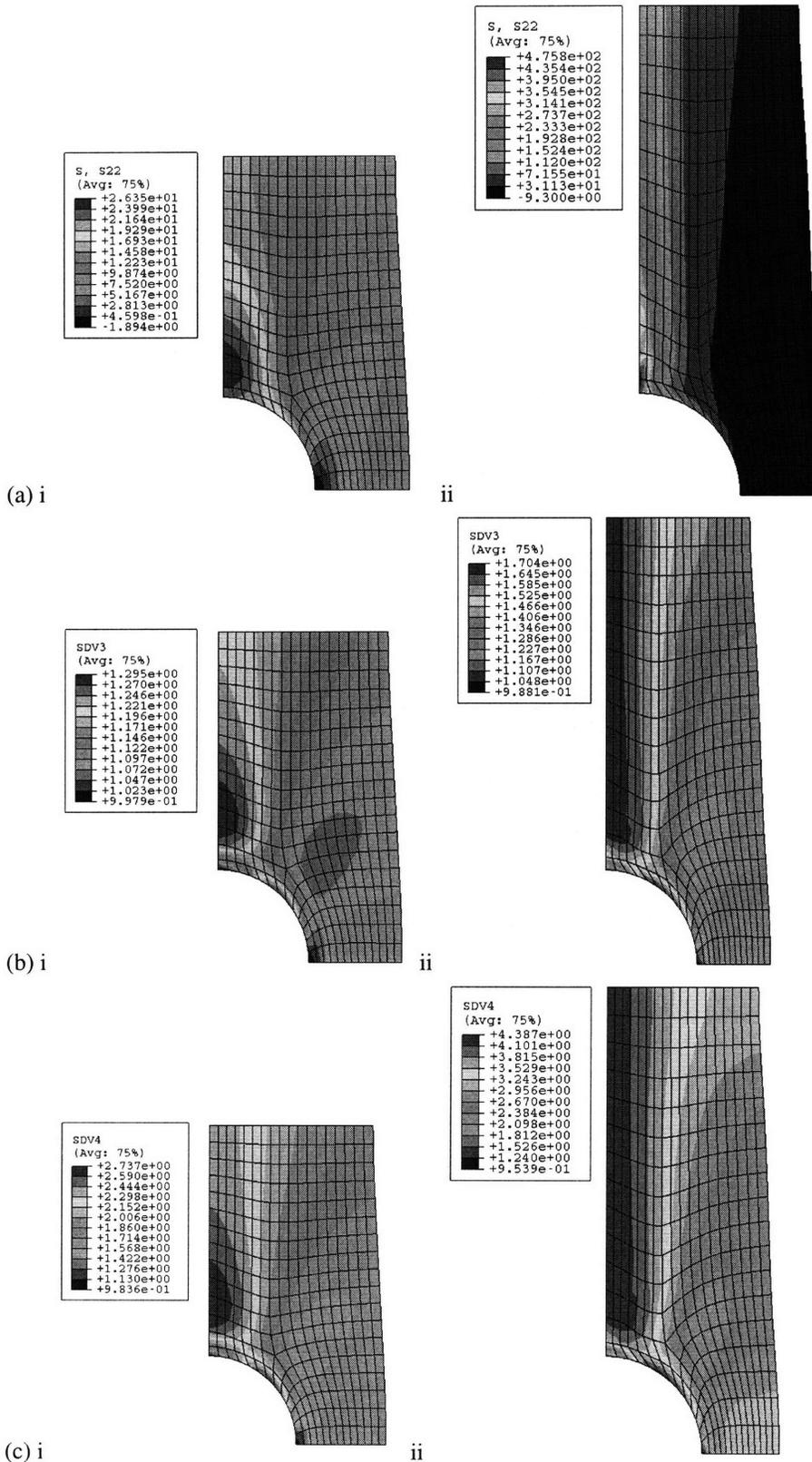


Figure 3.5 shows the contours for a volume fraction of 5% filler particle for (a) stress in the 22 direction, (b) the chain stretch and (c) the amplified chain stretch for the positions indicated on the graph at strains of (i) .5 and (ii) 1.

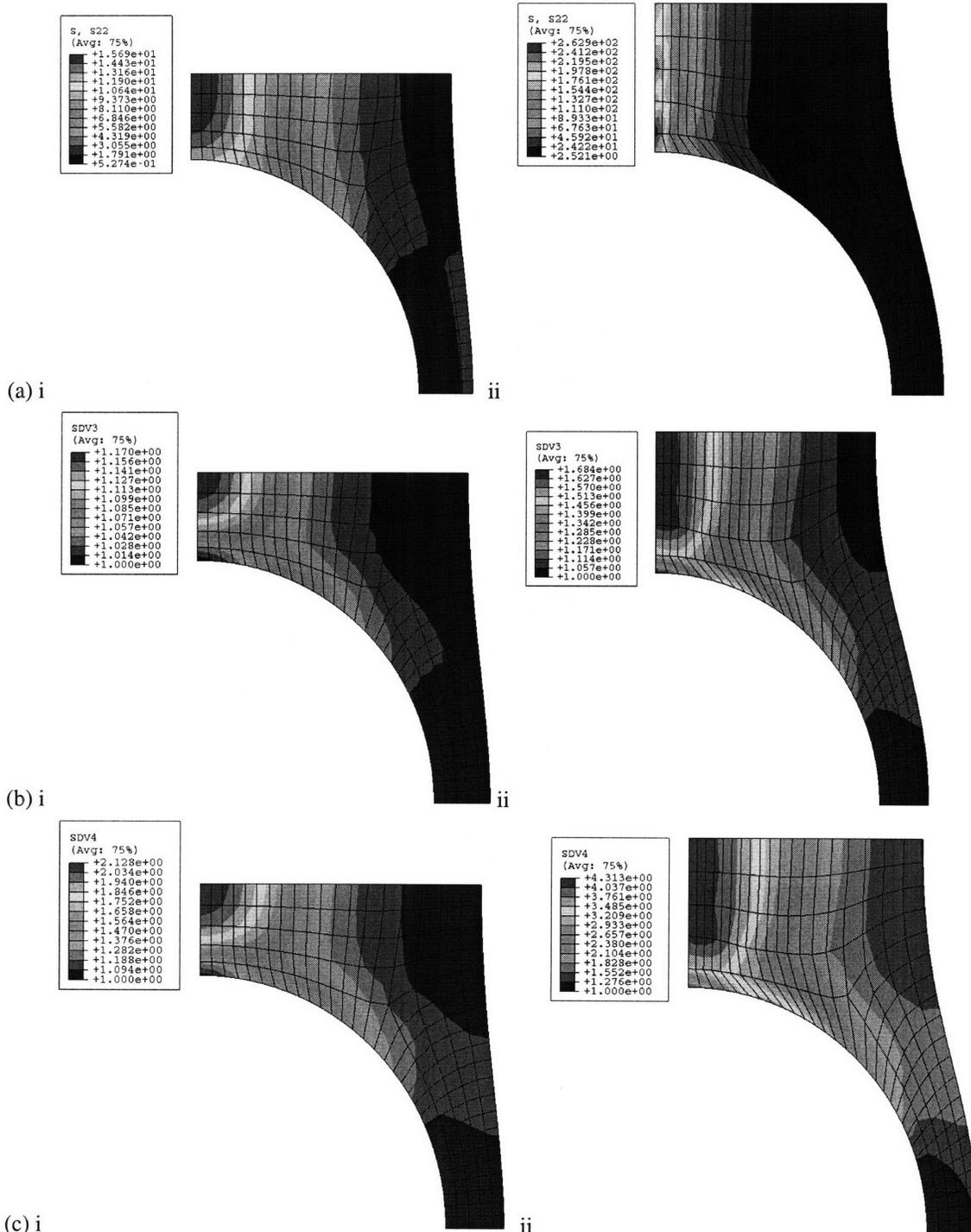


Figure 3.6 shows the contours for a volume fraction of 35% filler particle for (a) stress in the 22 direction, (b) the chain stretch and (c) the amplified chain stretch for the positions indicated on the graph at strains of (i) .1 and (ii) .3.

There is a dramatic dependence of the stress-strain curve on the volume fraction of filler particle, as seen in Figure 3.2. This is because the inclusion of a particle imposes additional constraints on how the material may stretch.

As the percentage of filler increases, the composite material becomes stiffer. Also, as the percentage of filler particles increases, the maximum strain allowed by the simulation decreases. This is due to geometrical constraints on the elements distorting the mesh in the simulation; as larger particles place a greater constraint on deformation

In general, stress is concentrated as expected. As seen in Figure 3.3, the stress is uniform throughout the element with no filler particle (Figure 3.3a); in the particle filled rubber, stress is concentrated in the matrix region along the particle, specifically where the particle and matrix meet, in the elements with filler particle. As the amount of filler particle increases, the stress becomes increasingly concentrated along the edge.

3.2 Effect of particle volume fraction on stress-strain behavior when matrix undergoes stretch-induced softening

The same analysis was performed, deforming elements as much as permitted by the simulation and then unloading them, this time including the effect of stretch-induced softening in the matrix behavior. The results are shown in Figure 3.7 and Figure 3.8, with specific cases highlighted in Figure 3.7. As with the case of no softening, the addition of filler particles made the material much stiffer, as compared to the case with no softening. However, in the cases where the matrix softens with strain, the enhancement in stiffness was much less than in the cases without softening. This is because more softening occurs in the filled rubber (after any level of macroscopic strain) which leads to the smaller enhancement for any given v_f .

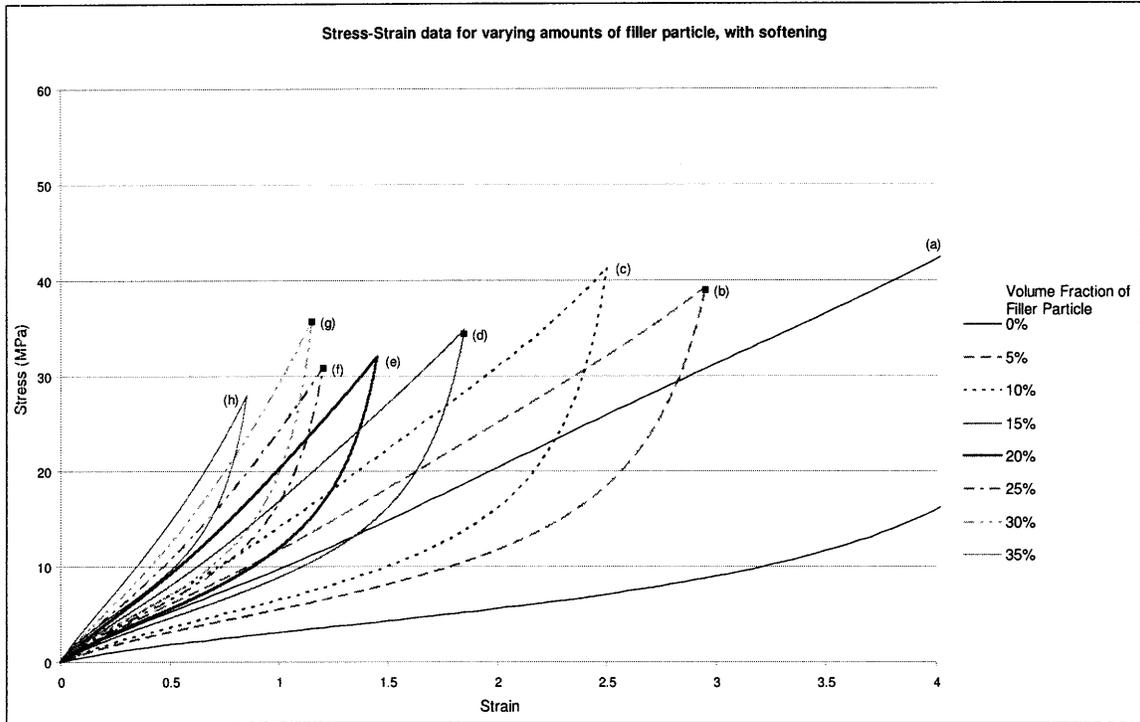
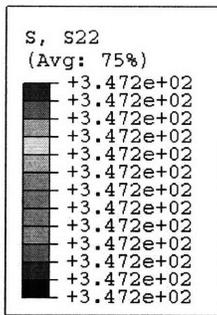
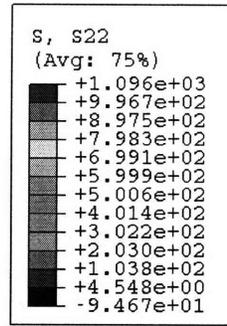


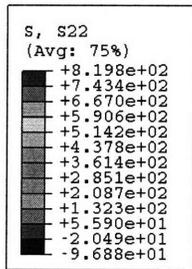
Figure 3.7 shows the stress-strain curves for the loading of rubber which undergoes softening with increasing volume fractions of filler particle.



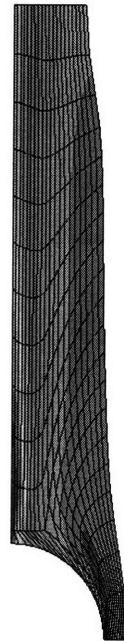
(a) 2



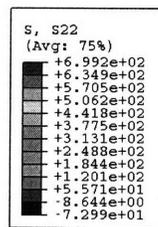
(b) 2



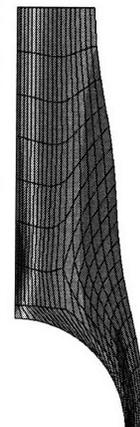
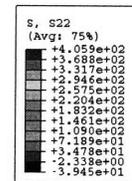
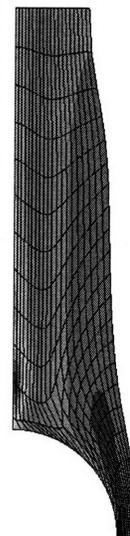
(c)



(d)



(e)



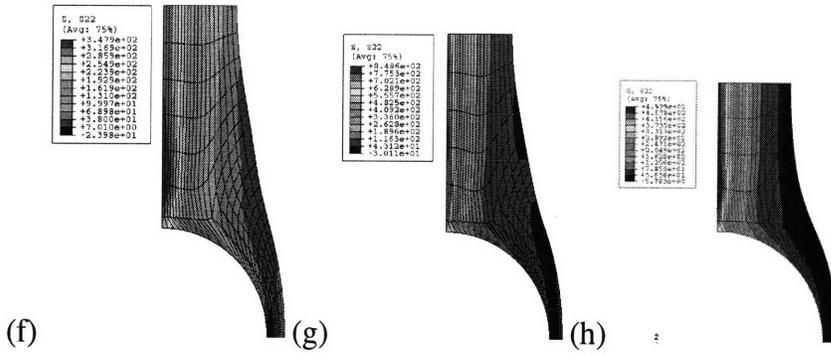


Figure 3.8 shows the stress distribution in the 22 direction for each of the positions indicated on the graph; (a) has no filler particle, (b) has 5% volume fraction of filler particle, and (c) has 35% volume fraction of filler particle.

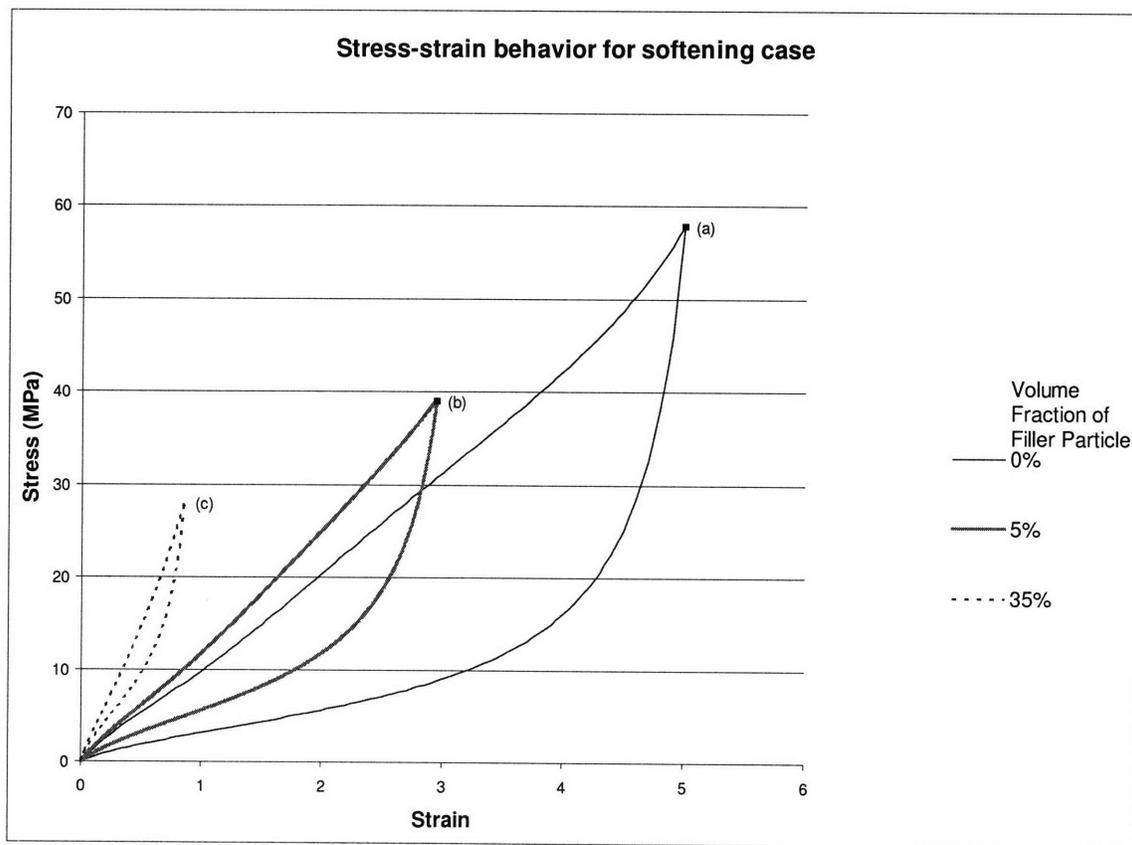
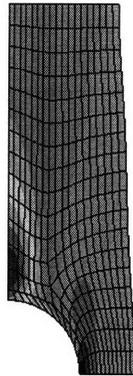
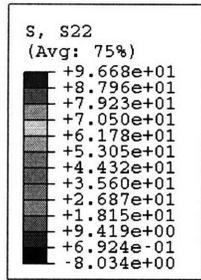
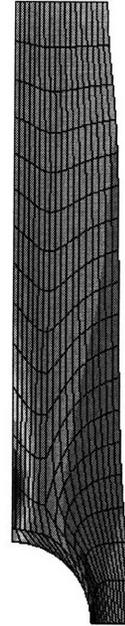
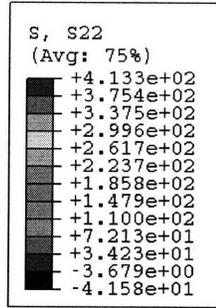


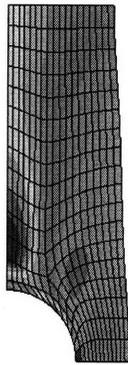
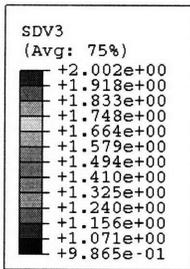
Figure 3.9 shows the stress-strain curves for rubber with 0%, 5%, and 35% filler particle.



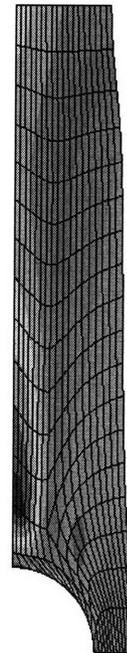
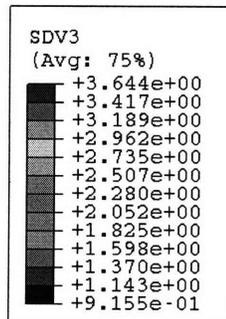
(a) i



ii



(b) i



ii

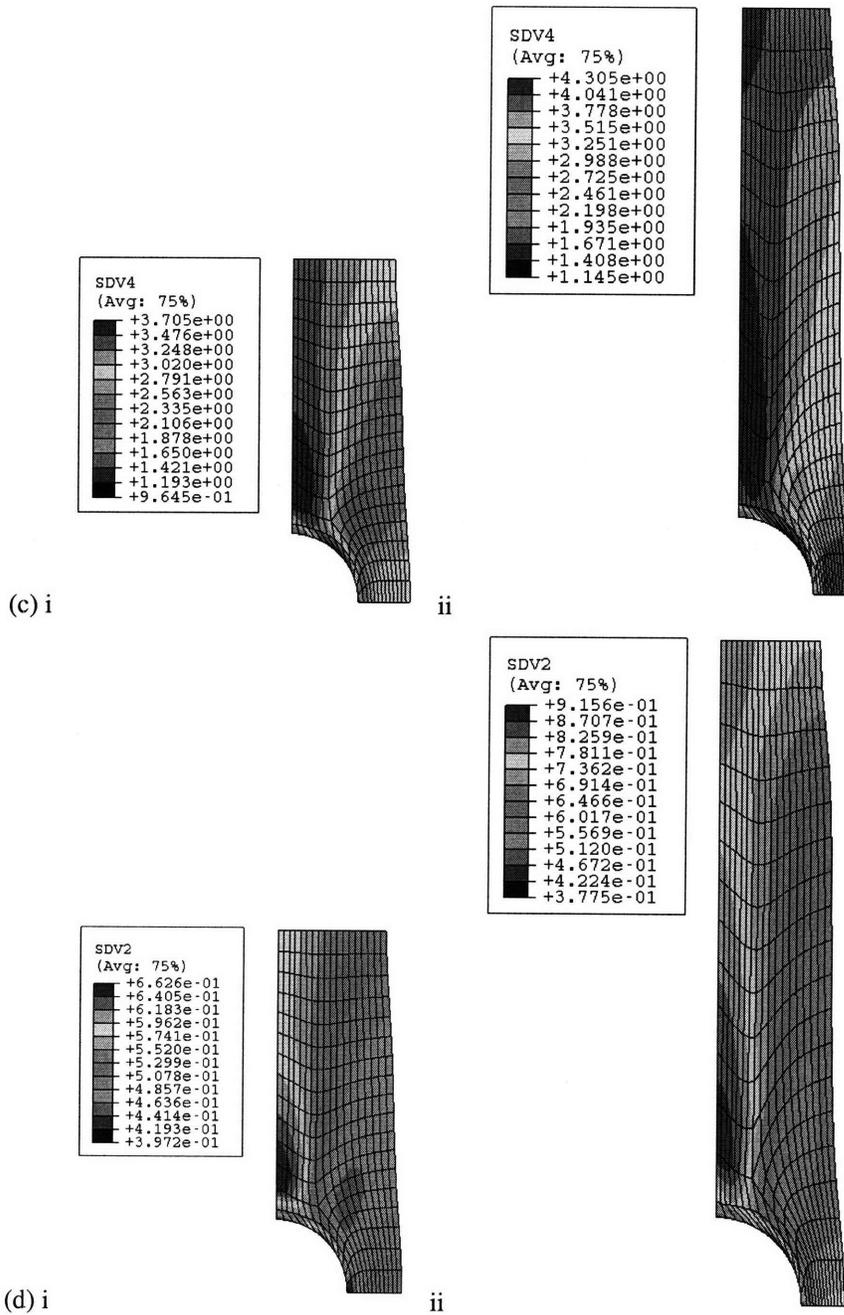
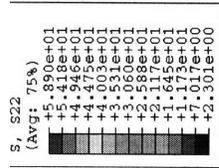
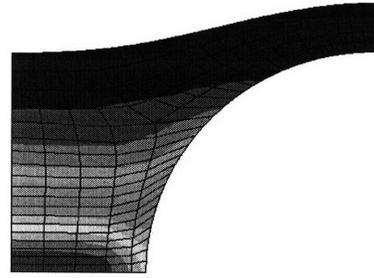


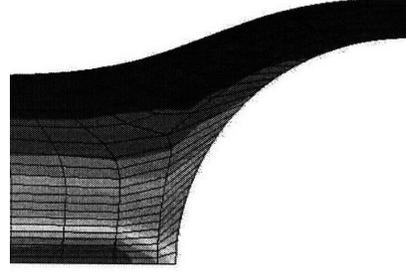
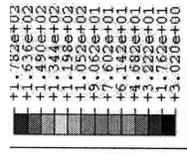
Figure 3.10 shows the contours for a volume fraction of 5% filler particle for (a) stress in the 22 direction, (b) the chain stretch (c) the amplified chain stretch and (d) the evolution of soft volume fraction for the positions indicated on the graph at strains of (i) 1.1 and (ii) 2.2.



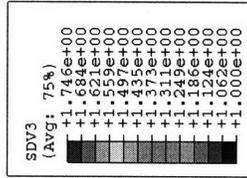
(a) i



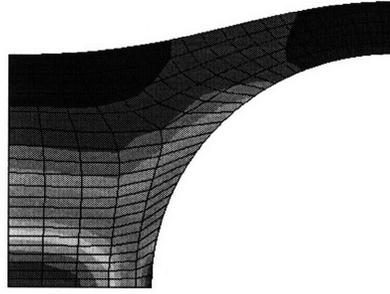
ii



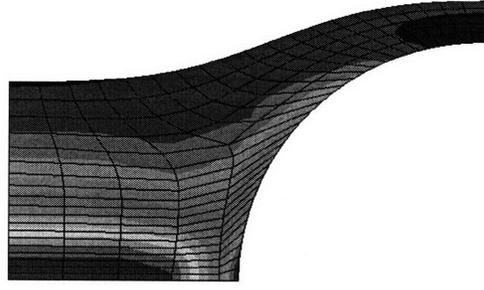
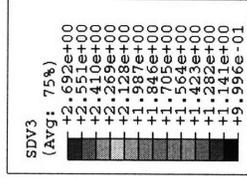
(a) ii



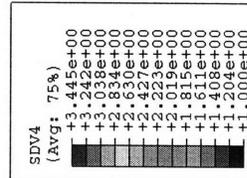
(b) i



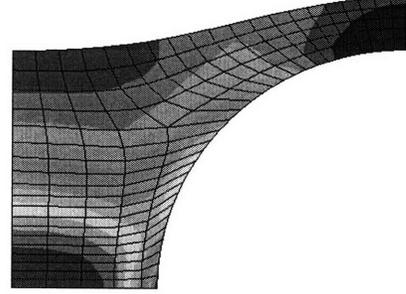
ii



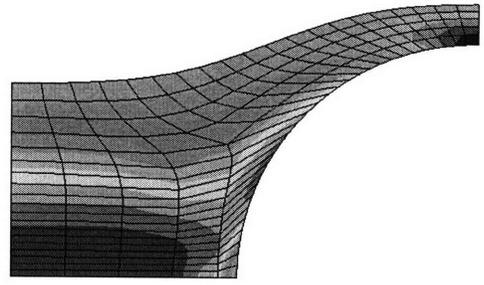
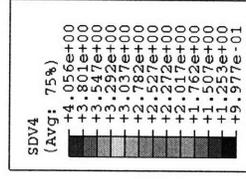
(b) ii



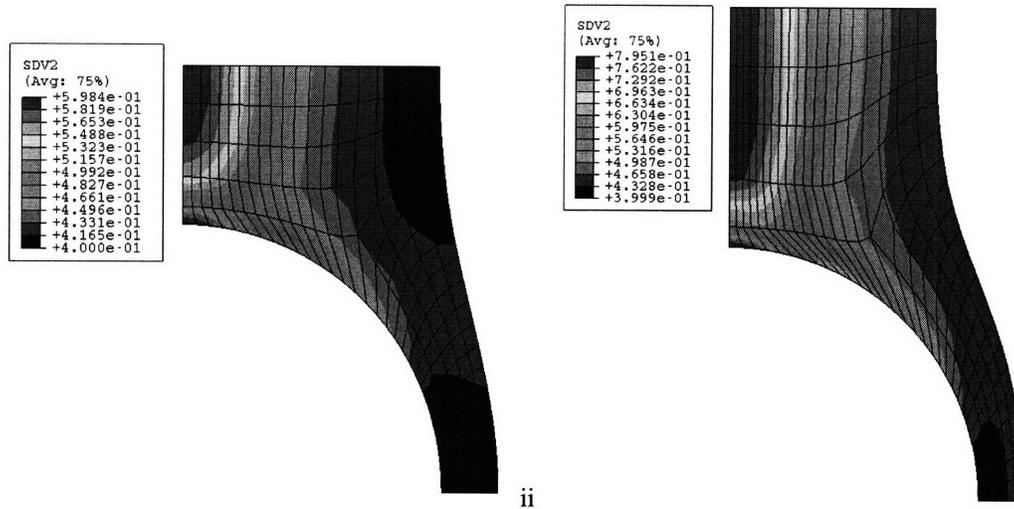
(c) i



ii



(c) ii



(d) i
 ii
 Figure 3.11 shows the contours for a volume fraction of 35% filler particle for (a) stress in the 22 direction, (b) the chain stretch (c) the amplified chain stretch and (d) the evolution of soft volume fraction for the positions indicated on the graph at strains of (i) .285 and (ii) .57.

Looking at contours of σ_{22} compared to the chain stretch and amplified chain stretch, as shown in Figure 3.10 for the 5% volume fraction case and in Figure 3.11 for the 35% volume fraction case, one notices that the highest values of stress and both chain stretches are found in similar locations: along the axis and directly above the particle. The chain stretch is an effective measure of deformation, so it is expected that the regions of greatest stress would also have a large value of chain stretch, and a large value of softening. This is found to be true; for the case of 5% volume fraction at a strain of 1.1, the location of the highest chain stretch corresponds to the location of greatest v_s , which is .66, compared with an average v_s value of .5 over the matrix. Similarly, for the 35% volume fraction case, at a strain of .57, the regions of greatest chain stretch and greatest v_s also correspond, and v_s is again significantly higher than the average value, reaching a level of .79 at the region of greatest chain stretch, compared to an average value of .49.

For a given applied strain, as seen in Figure 3.12, the size of the hysteresis curve increases with increased volume fraction of filler particle. This is a direct result of the

amplified level of strain in the matrix of the filled rubber giving more softening when compared to that of the unfilled rubber which in turn gives the observed increase in hysteresis.

For a given stress, as shown in Figure 3.13, the amount of strain needed to achieve this stress decreases as the volume fraction of filler particle increases. A comparable level of hysteresis is observed for the cases of v_f at this applied strain.

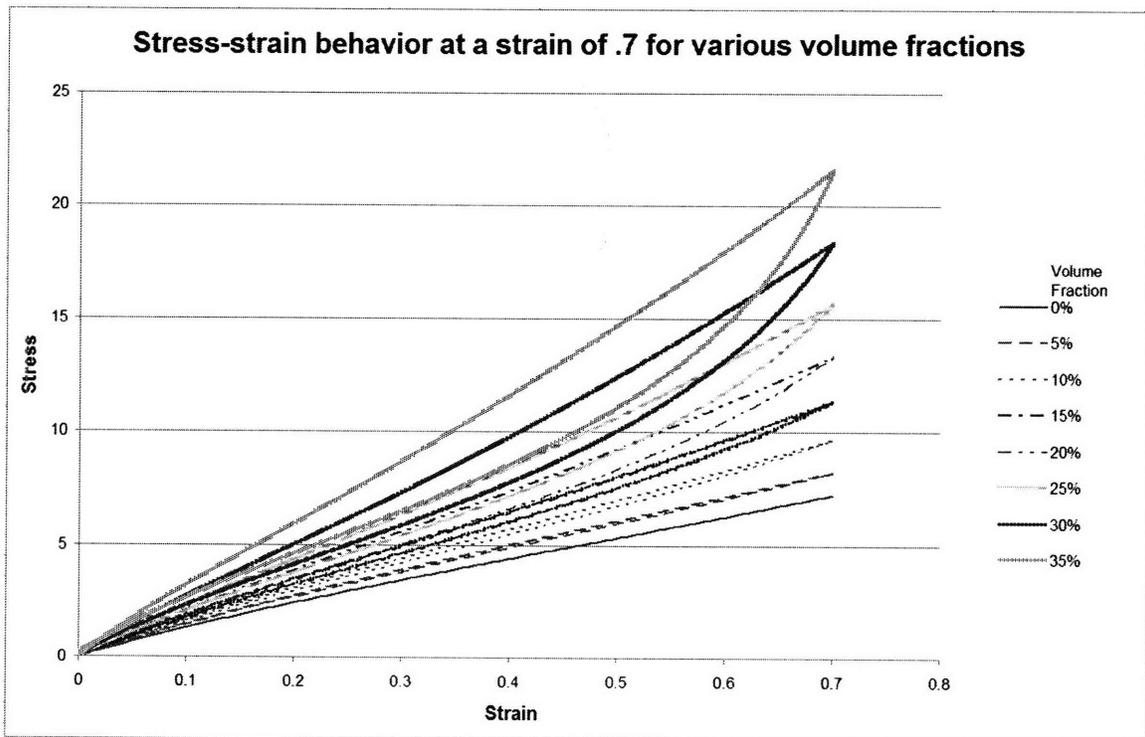


Figure 3.12 shows the stress-strain behavior for the different volume fractions of filler particle loaded to a strain of .7. As the amount of filler increases, so does the size of the hysteresis curve.

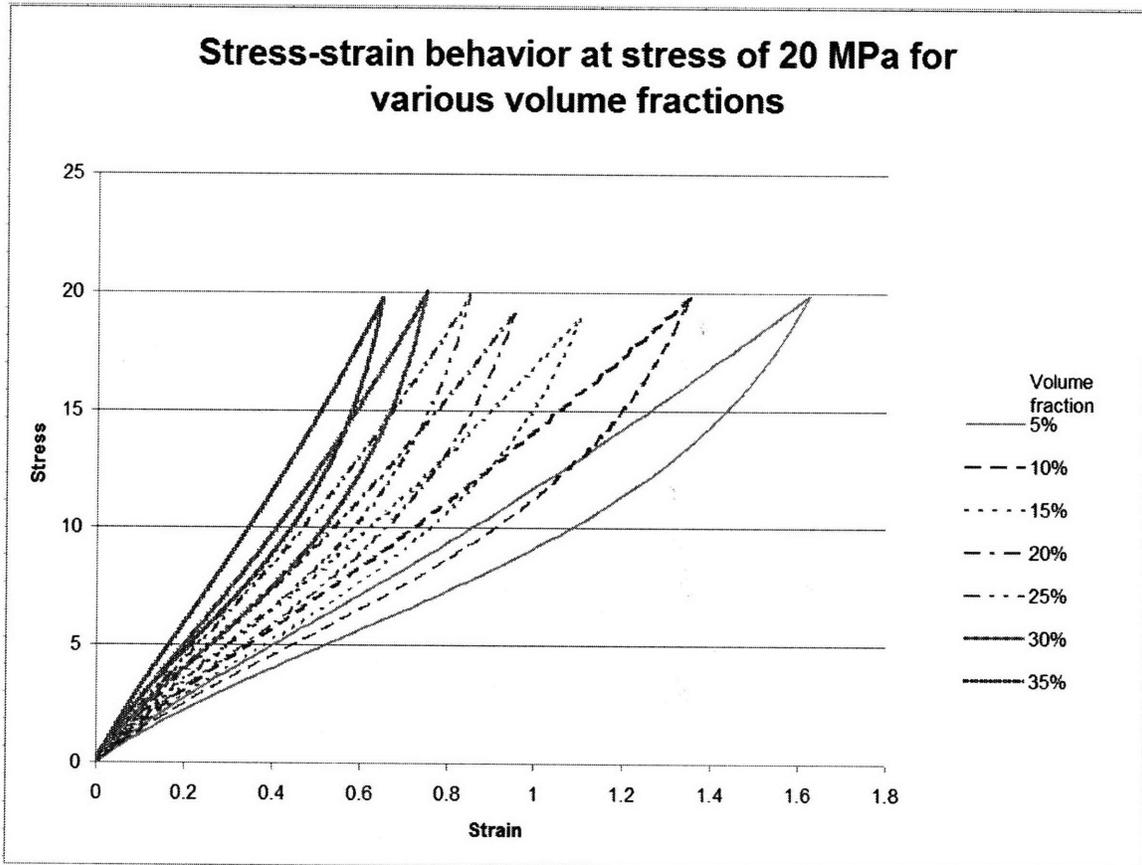


Figure 3.13 shows the stress-strain behavior for the different volume fractions of filler particle loaded to a stress of 20 MPa. As the volume fraction of filler increases, the strain needed to reach the given stress level decreases.

Comparing the cases of softening versus no softening, in Figure 3.14, it can be seen that in the cases where softening occurred, much larger strains were possible, as the material had a lower stiffness.

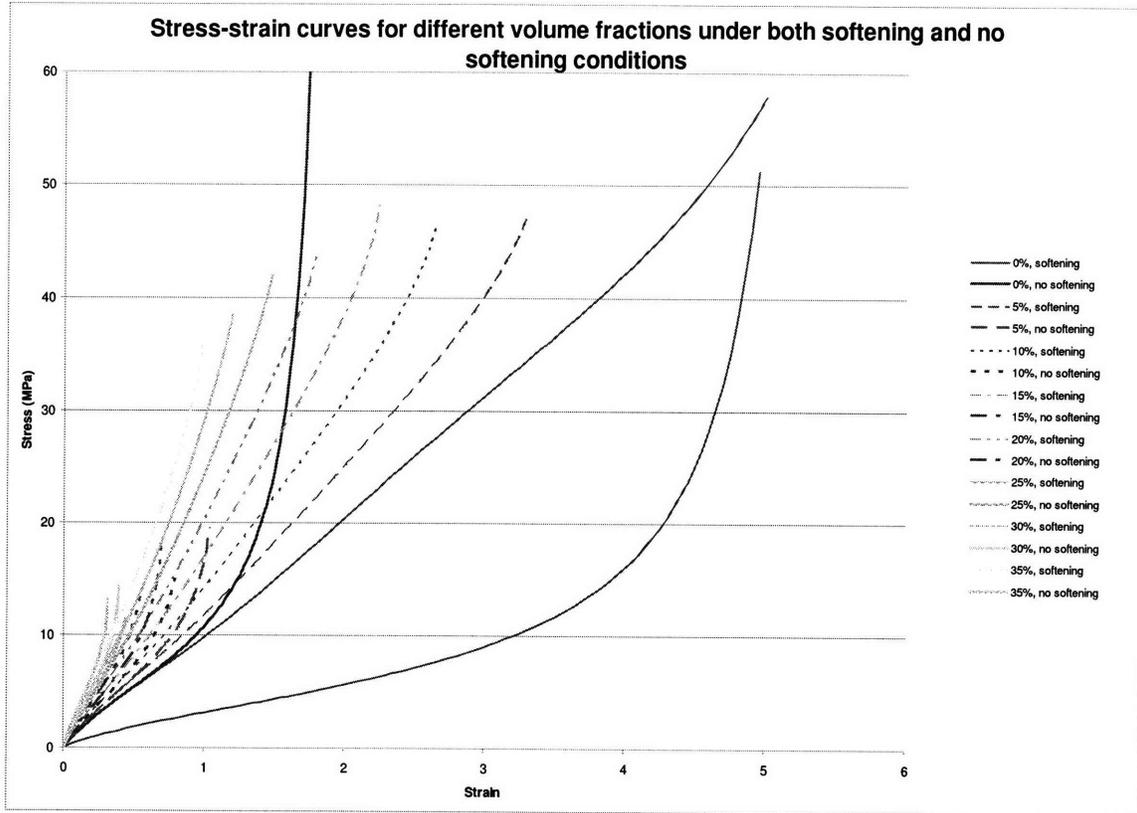
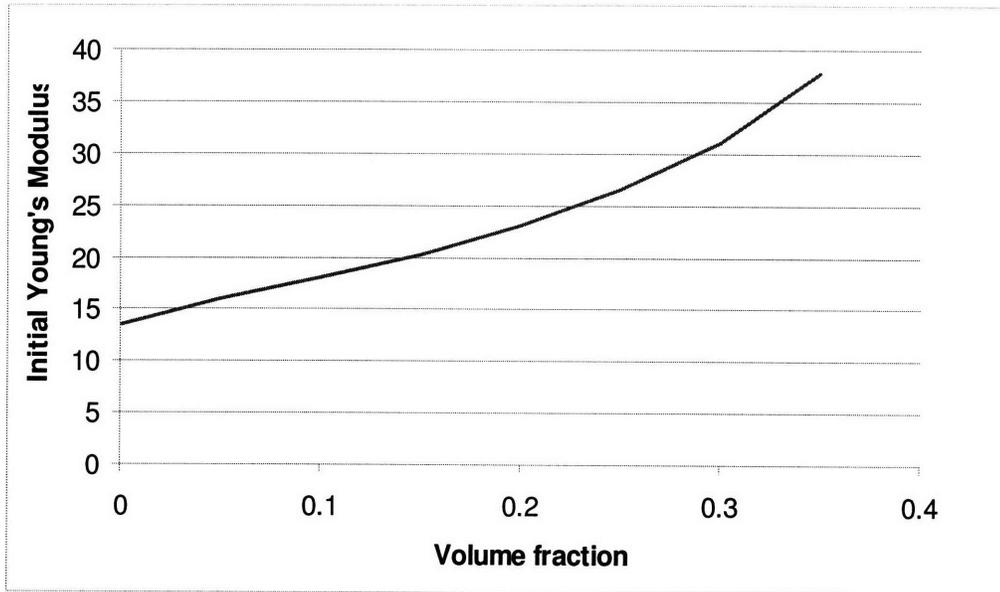
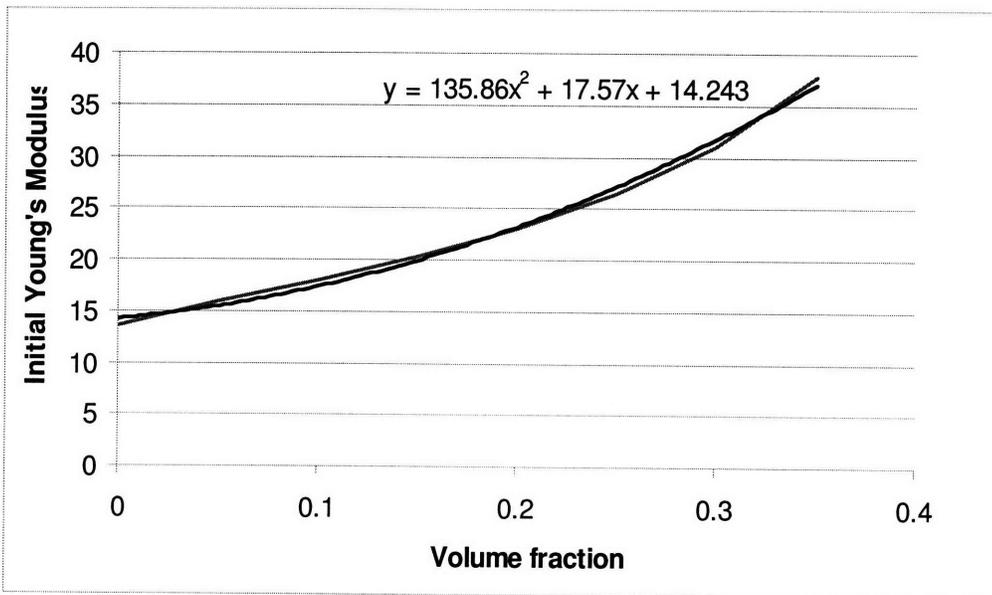


Figure 3.14 shows the comparison of stress and strain curves for both softening and no softening cases with different amounts of filler particle.

As with the case with no softening, as the percentage of filler increases, the stiffness increases, as illustrated in the following graph of percentage filler versus Young's Modulus, Figure 3.15. The amount of filler particle appears to have a quadratic relationship to the initial Young's Modulus, given by the equation $E = 135.86v_f^2 + 17.57v_f + 14.243$, where v_f is the volume fraction of filler particle.



(a)



(b)

Figure 3.15 (a) shows the initial Young's Modulus of the material as a function of volume fraction for the case with softening. (b) shows a trendline for the chart and a possible function for the initial Young's Modulus of the material as a function of the volume fraction of filler particle.

The stiffening behavior can also be seen in a comparison of volume fraction to strain level for varying fixed levels of stress, shown in Figure 3.16.

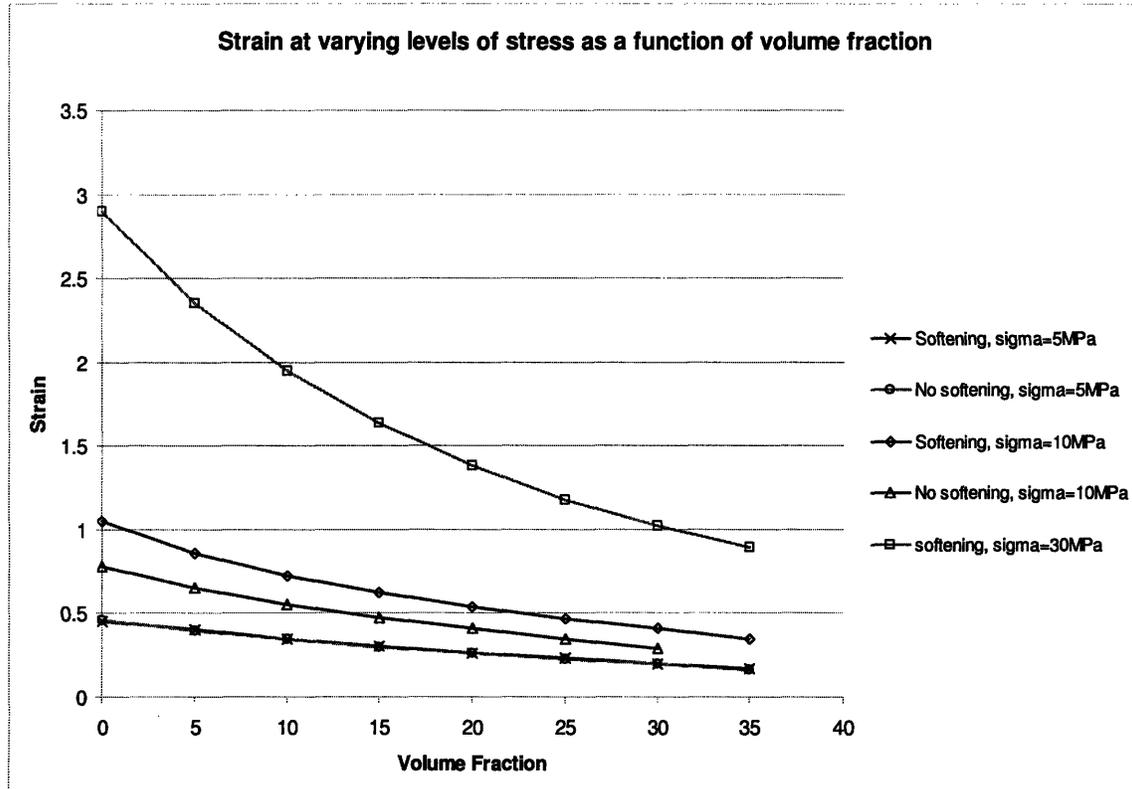


Figure 3.16 shows the strain level as a function of volume fraction, for stress levels $\sigma=5\text{MPa}$ (both softening and no softening), $\sigma=10\text{MPa}$ (both softening and no softening), and $\sigma=30\text{MPa}$ (only softening).

For low stress levels, there is very little difference between the softening and no softening cases. This difference increases at greater stress levels. This graph again shows the overall trend that as volume fraction increases, lower strain levels produce the same amount of stress, and the difference between strain level needed to achieve a given stress increases at higher stress levels.

The comparison of volume fraction to stress levels for given levels of strain was also examined, and the results are shown in Figure 3.17. At low strain levels, the difference between the softening and no softening conditions is low. At increasing strain levels, the difference becomes increasingly pronounced. As seen before, as volume

fraction increases, the level of stress at a given strain increases.

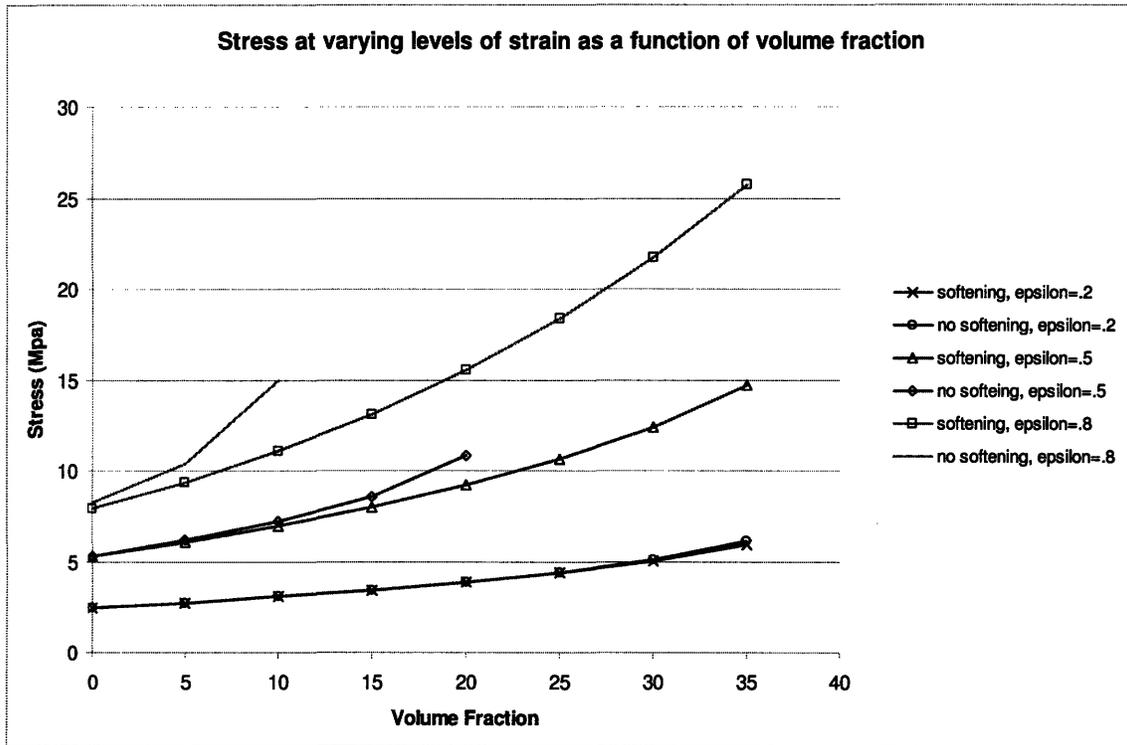


Figure 3.17 shows the stress level as a function of volume fraction, for strain levels $\epsilon=.2$ (both softening and no softening), $\epsilon=.5$ (both softening and no softening), and $\epsilon=.8$ (both softening and no softening).

For this analysis, the evolution of the volume fraction of soft material was also examined, as shown in Figure 3.18.

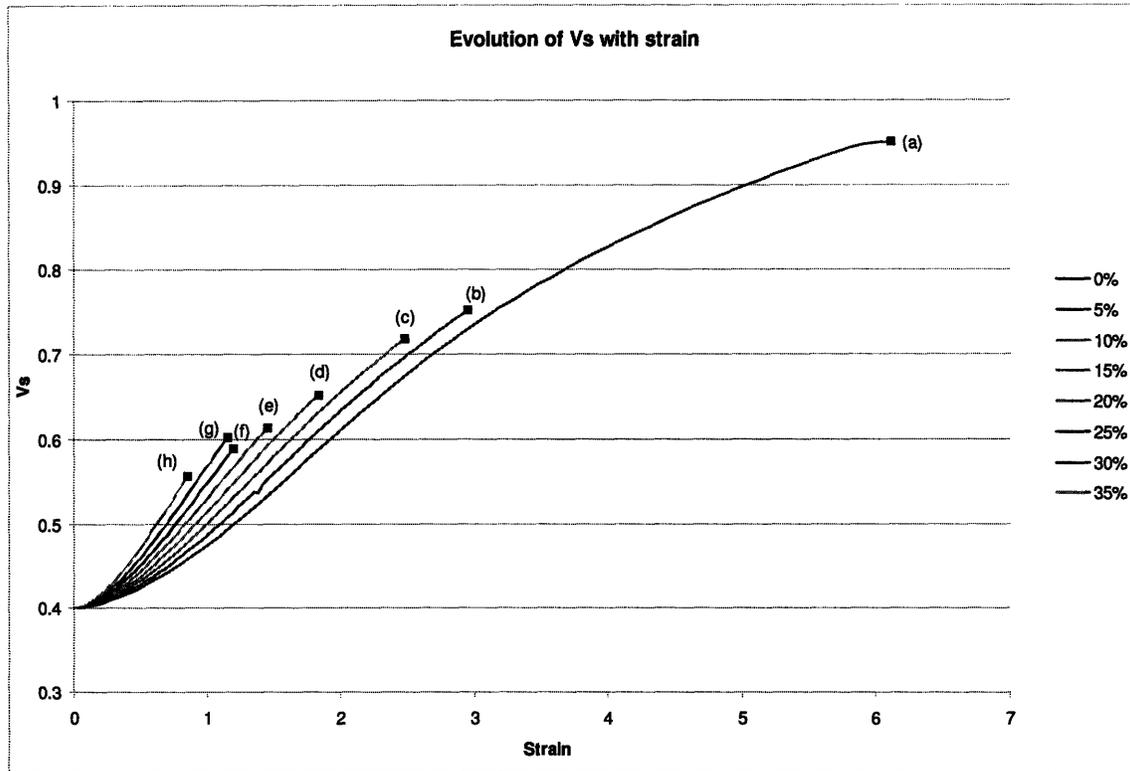


Figure 3.18 shows the evolution of “average” soft volume fraction (averaged over all matrix), where some regions of matrix experience much greater softening than average with time, and some regions do not soften at all, with increasing strains for increasing volume fraction of filler particles.

The value for v_s shown is the average over the matrix. The value was determined by taking a weighted average, using the value of v_s at each integration point and the volume represented by that integration point. As seen in the figure, the evolution of softening with respect to macroscopic strain increases dramatically as the volume fraction of filler particle increases. When filler particles are added, the evolution of v_s in specific locations also changes dramatically. v_s evolves uniformly in the material with no filler particle, but varies over the element with filler particle. When the material is loaded to the same strain, the level of v_s reached increases with increasing volume fraction, as seen in Figure 3.21.

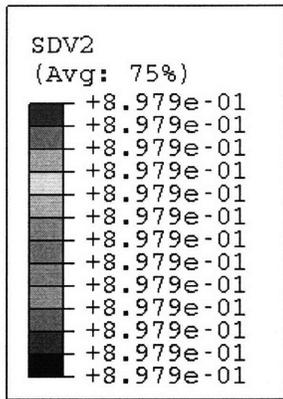


Figure 3.19 shows the softening behavior for a material with no filler particle. In this case, the softening is uniform. This case corresponds to location (a) in the graph shown in Figure 3.18.

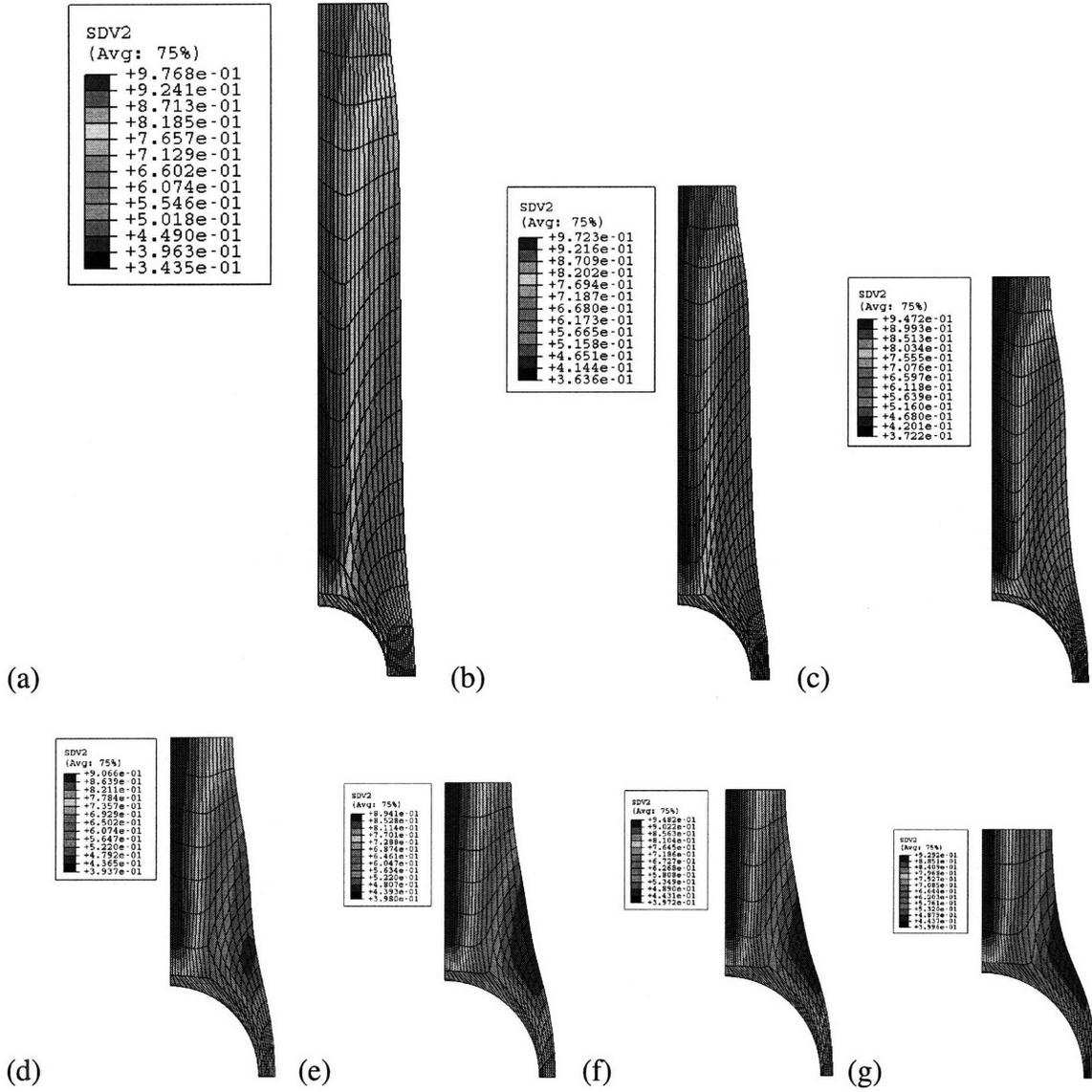


Figure 3.20 shows the softening behavior for increasing volume fractions of filler particle: (a) 5%, (b) 10%, (c) 15%, (d) 20%, (e) 25%, (f) 30%, (g) 35%. In these cases, softening is not uniform.

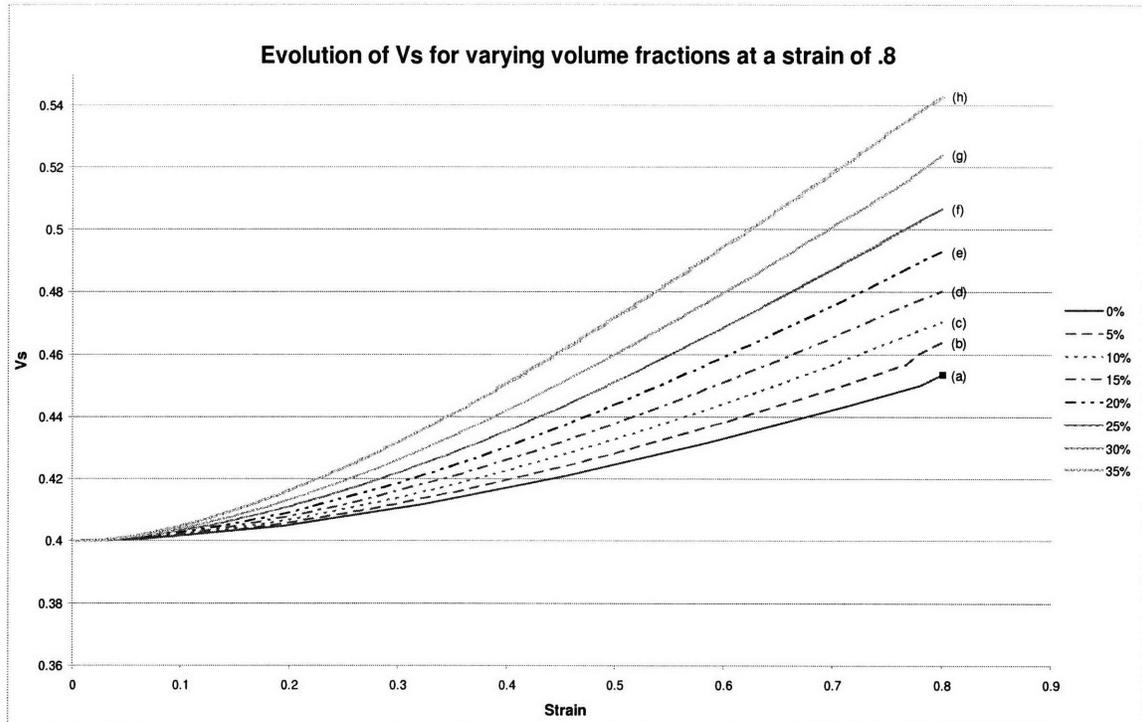


Figure 3.21 shows the evolution of the soft volume fraction for different cases of v_f . As volume fraction increases, so does the level of v_s attained at a given strain.

For each volume fraction, unloading and reloading to various strain levels was also examined, as shown in Figure 3.22. For low volume fractions of filler particles, little difference was seen as the material was repeatedly loaded and unloaded; for larger volume fractions, softening increased with loading and unloading. As before, the maximum strain to which an element could be loaded decreases as volume fraction increases, due to limits of the simulation.

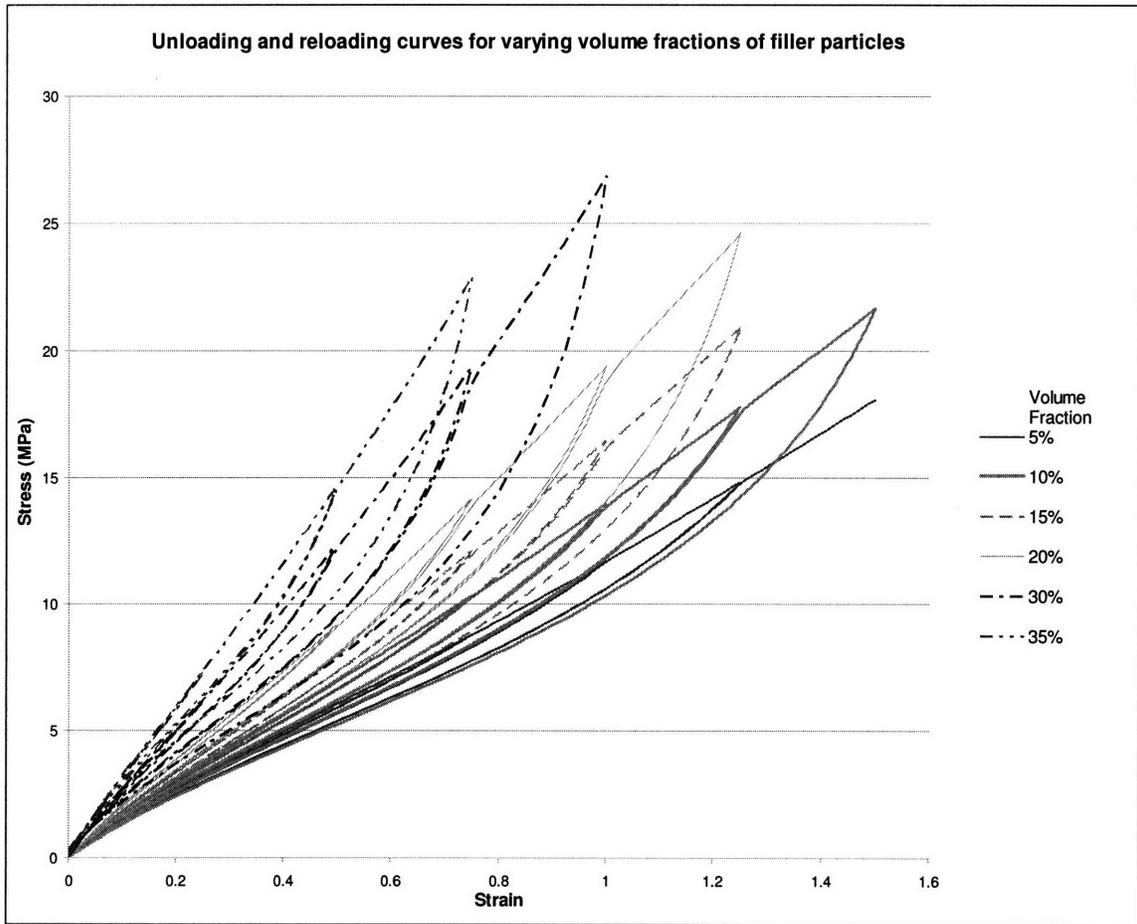


Figure 3.22 shows the loading and unloading curves for repeated loading of the different volume fractions of filler particle.

The results for loading and unloading for each case of v_f are shown in Figure 3.23. As seen before in the graph of the model, when the material is reloaded, it follows the unloading curve of the previous cycle until the strain exceeds the previous maximum strain, at which point the loading curve rejoins the main curve. The distribution of stresses across the element can be seen in Figure 3.24.

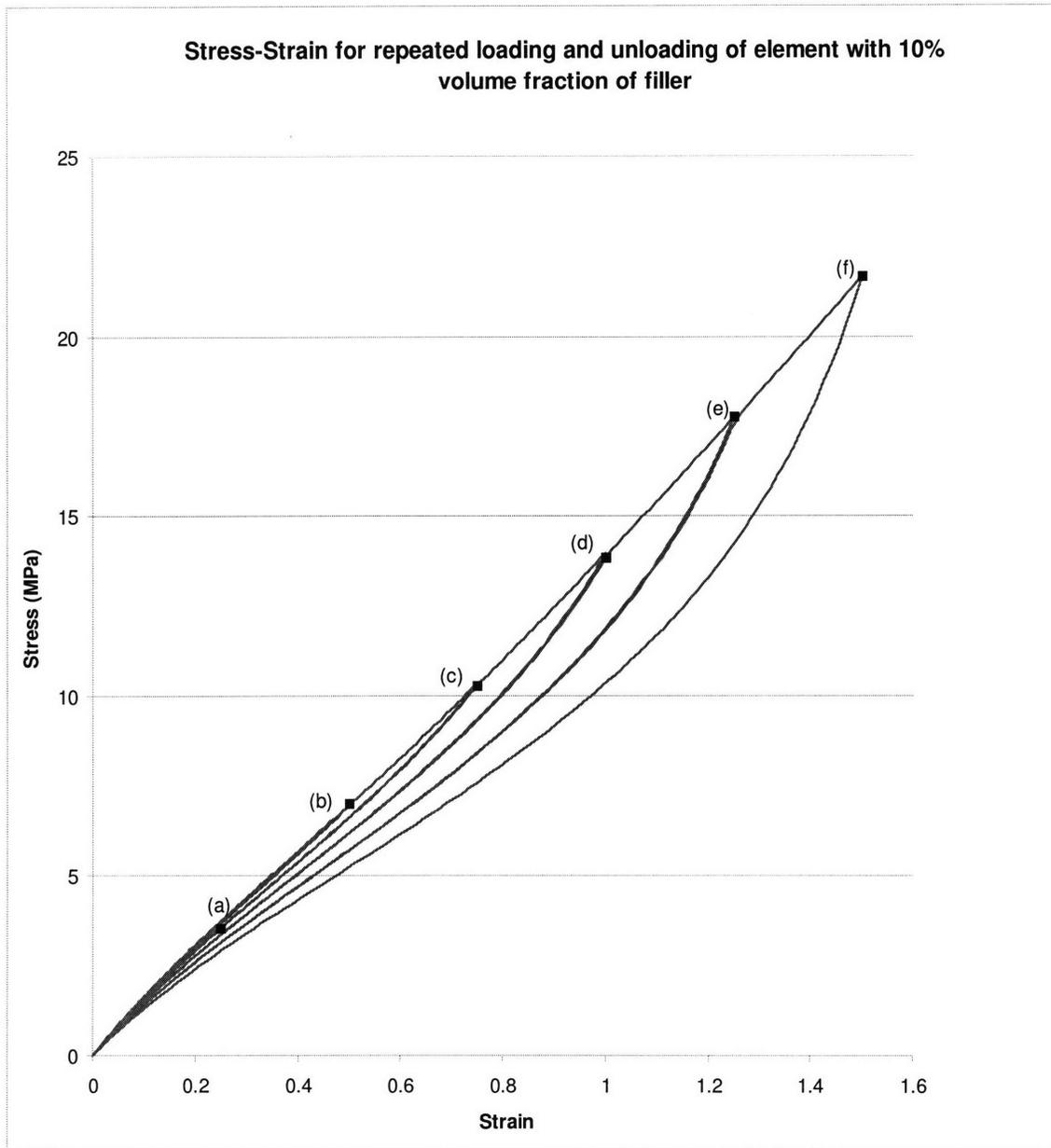


Figure 3.23 shows the stress-strain behavior for an element with 10% volume fraction of rigid filler particle which was loaded and unloaded six times to increasing levels of strain.

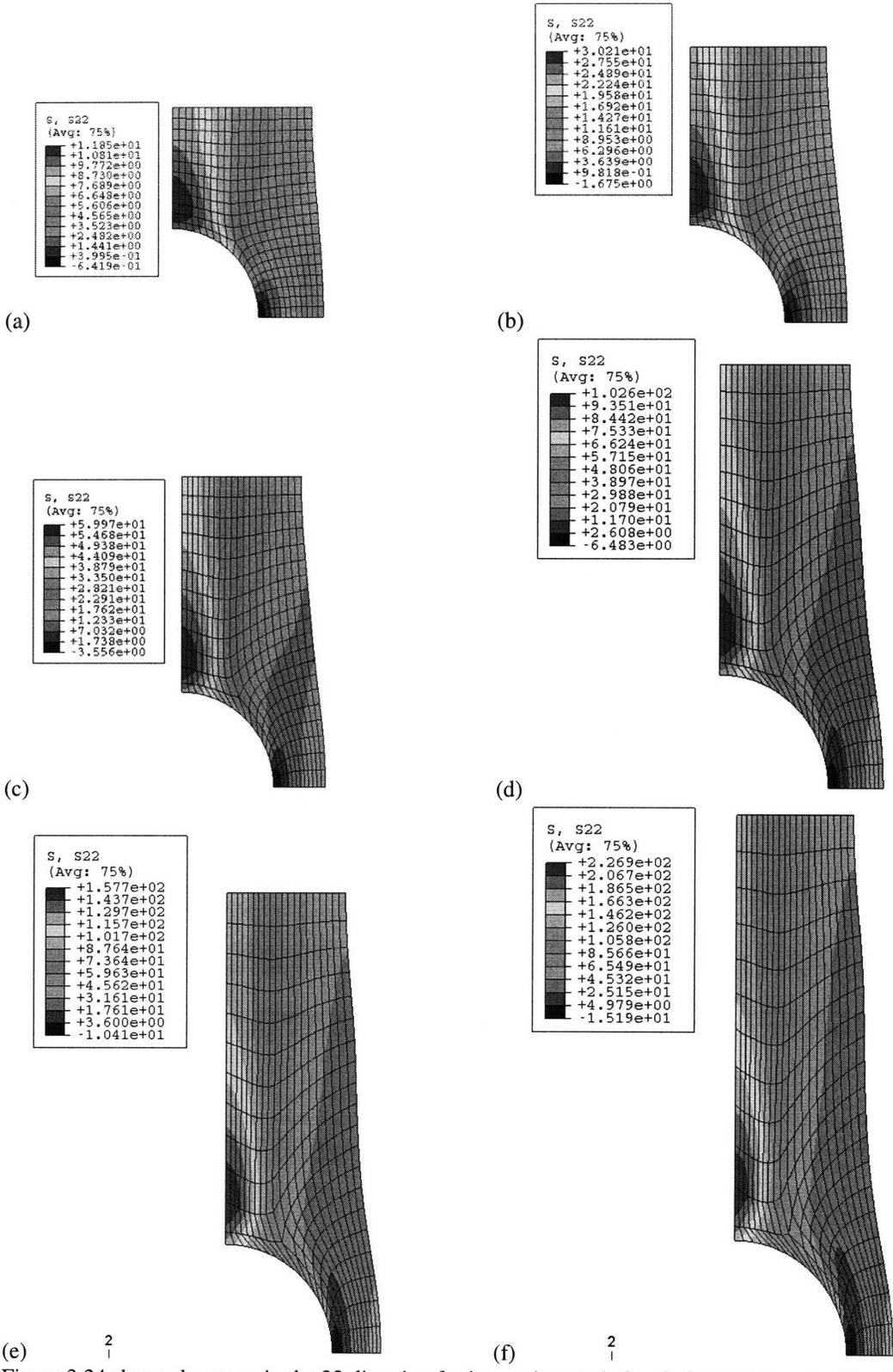


Figure 3.24 shows the stress in the 22 direction for increasing strain levels for an element with a 10% volume fraction of filler particle. (a) is at a strain level of .25, (b) is at a strain level of .5, (c) is at a strain level of .75, (d) is at a strain of 1, (e) is at a strain of 1.25, and (f) is at a strain of 1.5

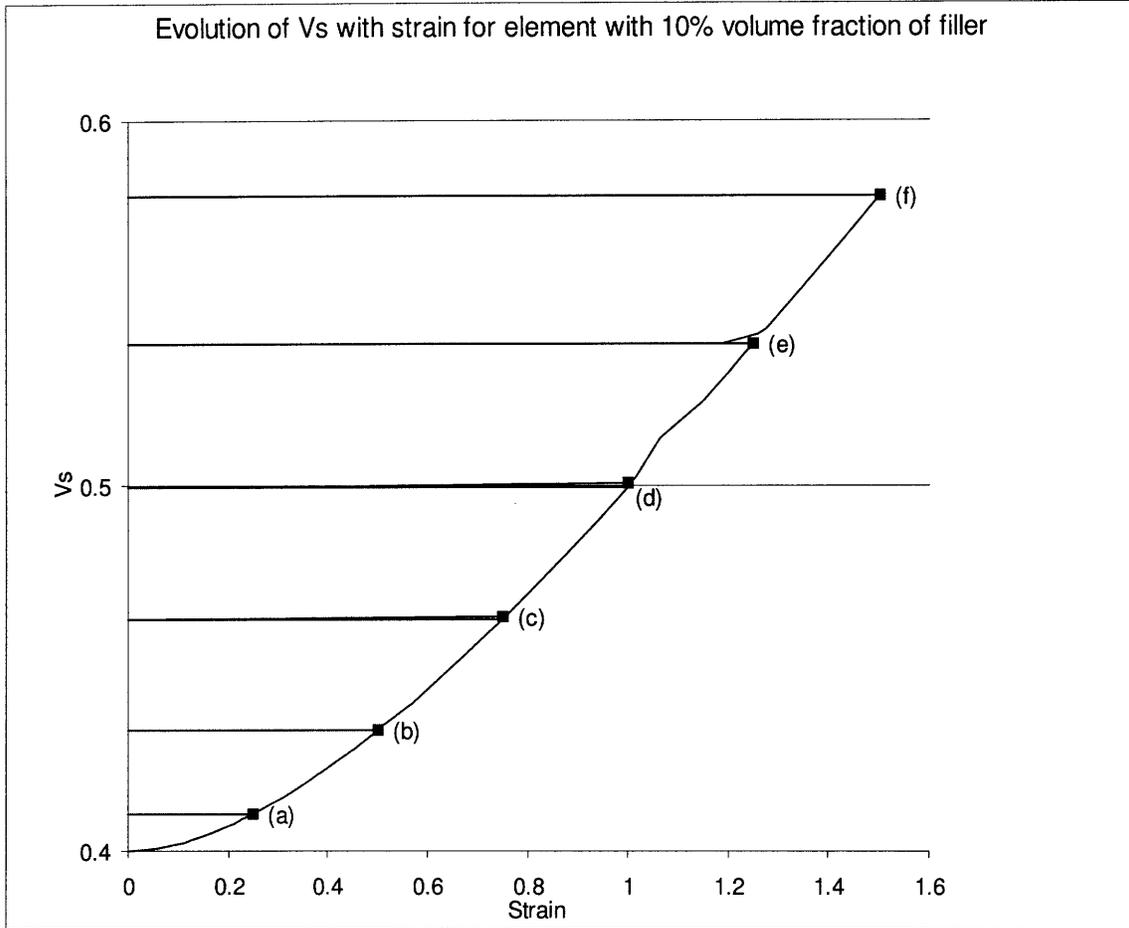
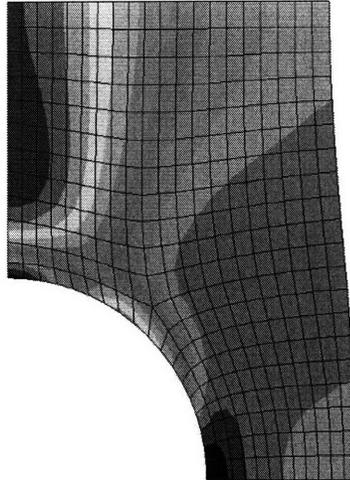
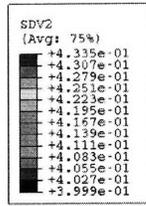
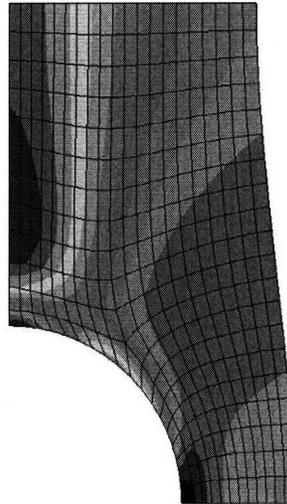
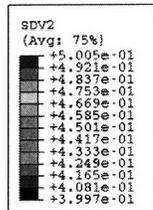


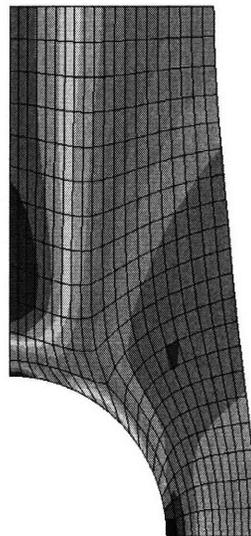
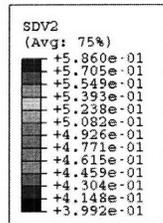
Figure 3.25 shows the evolution of the average v_s for the case with 10% volume fraction of rigid filler particle which was loaded and unloaded six times to increasing levels of strain.



(a) 2
1



(b) 2
1



(c) 2
1

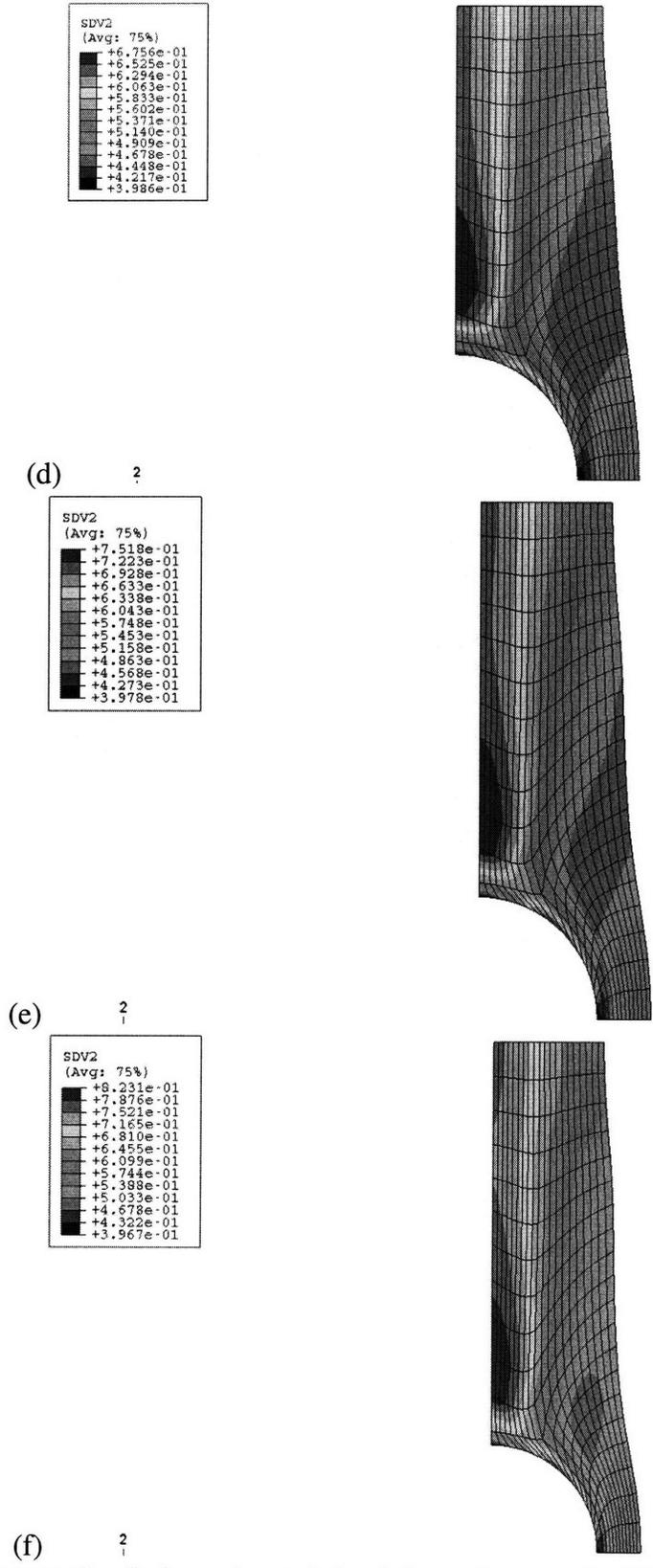


Figure 3.26 shows contours of v_s for increasing strain levels for an element with a 10% volume fraction of filler particle. (a) is at a strain level of .25, (b) is at a strain level of .5, (c) is at a strain level of .75, (d) is at a strain of 1, (e) is at a strain of 1.25, and (f) is at a strain of 1.5

Comparing the average v_s and the v_s at different points in the model, there are some significant differences. The average v_s only reaches a level of .58 (as seen in Figure 3.25), while the v_s in specific locations goes as high as .82 (as seen in Figure 3.26). The greater volume fraction of soft material is concentrated along the 2-axis of the element. In other areas, for instance, near the inclusion at the bottom of the element, v_s does not evolve at all. Thus, the inclusion of a rigid filler particle amplifies strain in different regions of the matrix and constrains strain in other regions of the matrix, leading to a strong distribution in the volume fraction of soft domain; in the unfilled rubber, v_s evolves uniformly as the material deforms.

3.3 Effects of occluded region on matrix

The results obtained from applying the micromechanical model to the filled rubber shown in Figure 3.27, do not correspond perfectly to the Harwood and Payne data; the behavior given by the model is less stiff than the behavior of the actual rubber.

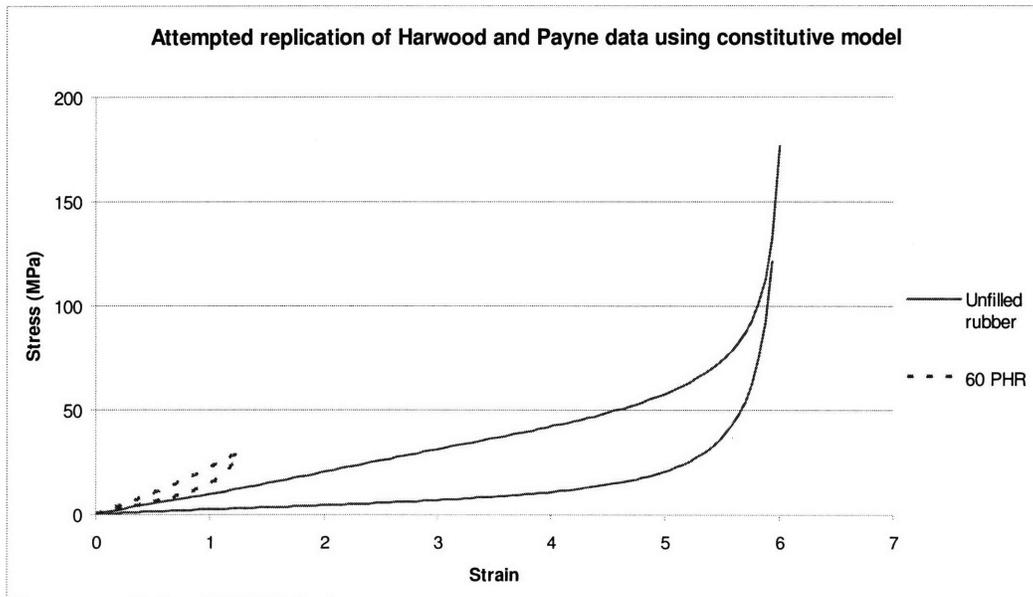
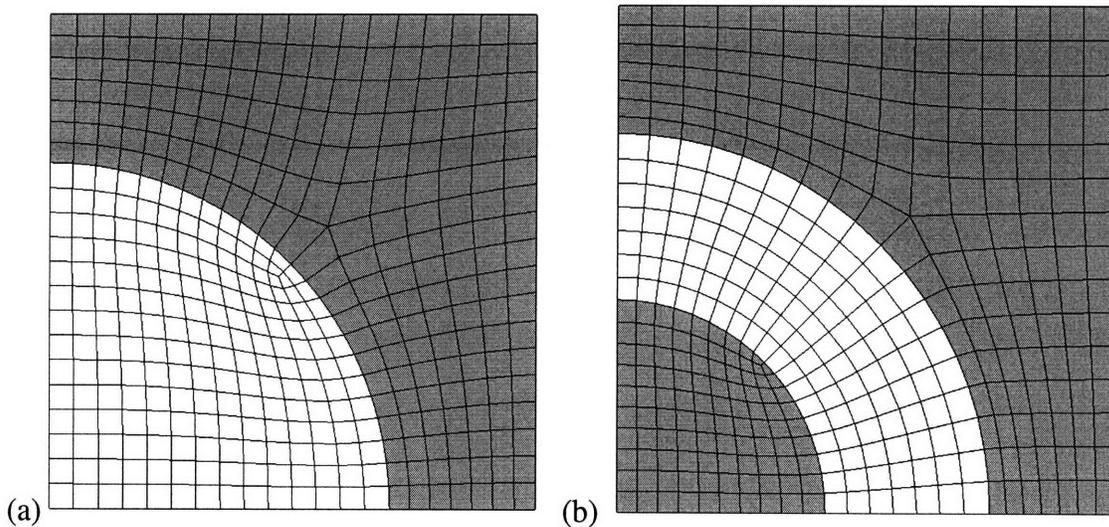


Figure 3.27 shows an attempt to replicate the Harwood and Payne data using the model previously described. The model is a reasonable fit for the unfilled rubber, but the behavior of the filled rubber in the paper is much stiffer than the behavior given by the model.

One reason for the different results may be the effects of occluded rubber. Prior to deformation, rubber may be trapped within groups of filler particles. This ‘occluded volume’ can result in the effective volume fraction of stiff particles being larger than the physical fraction. The effects of occluded regions of the matrix were also examined in order to see if the presence of occluded material might account for the difference seen between the results from the model and that from the Harwood and Payne data. To see the effect of the occluded volume, a model was created which simulated the effects of occlusion by surrounding a part of the matrix with a spherical shell with a Young’s Modulus of 1GPa and a Poisson’s ratio of .25, to simulate a necklace type structure of filler particles. Several volume fractions of occluded filler particle were tested, shown in Figure 3.28.



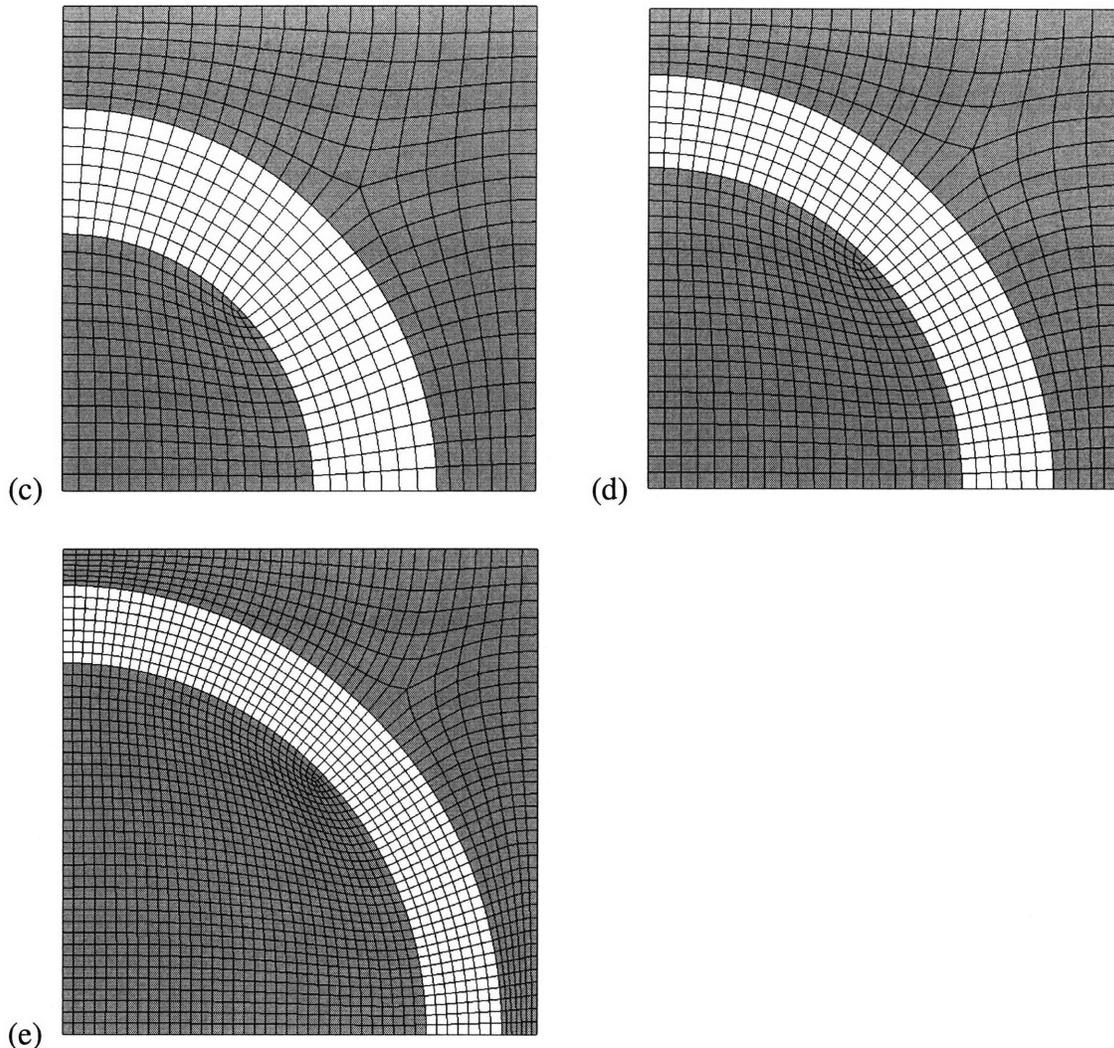


Figure 3.28 shows the initial mesh for a 23% volume fraction of filler particle (indicated in white) with varying amounts of occluded rubber: (a) has 0% occluded, (b) has 5% occluded, (c) has 10% occluded, (d) has 20% occluded, and (e) has 30% occluded.

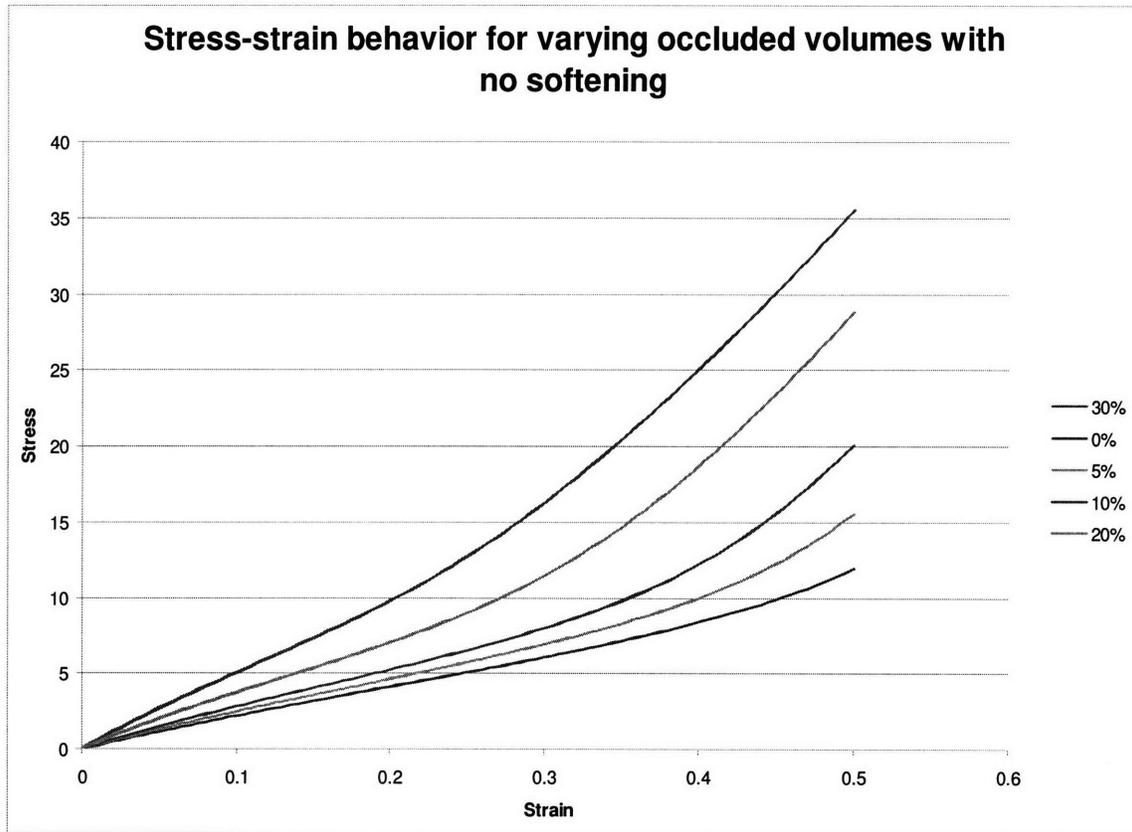


Figure 3.29 shows the stress-strain behavior for increasing volume fractions of occluded material when there is no softening of the matrix.

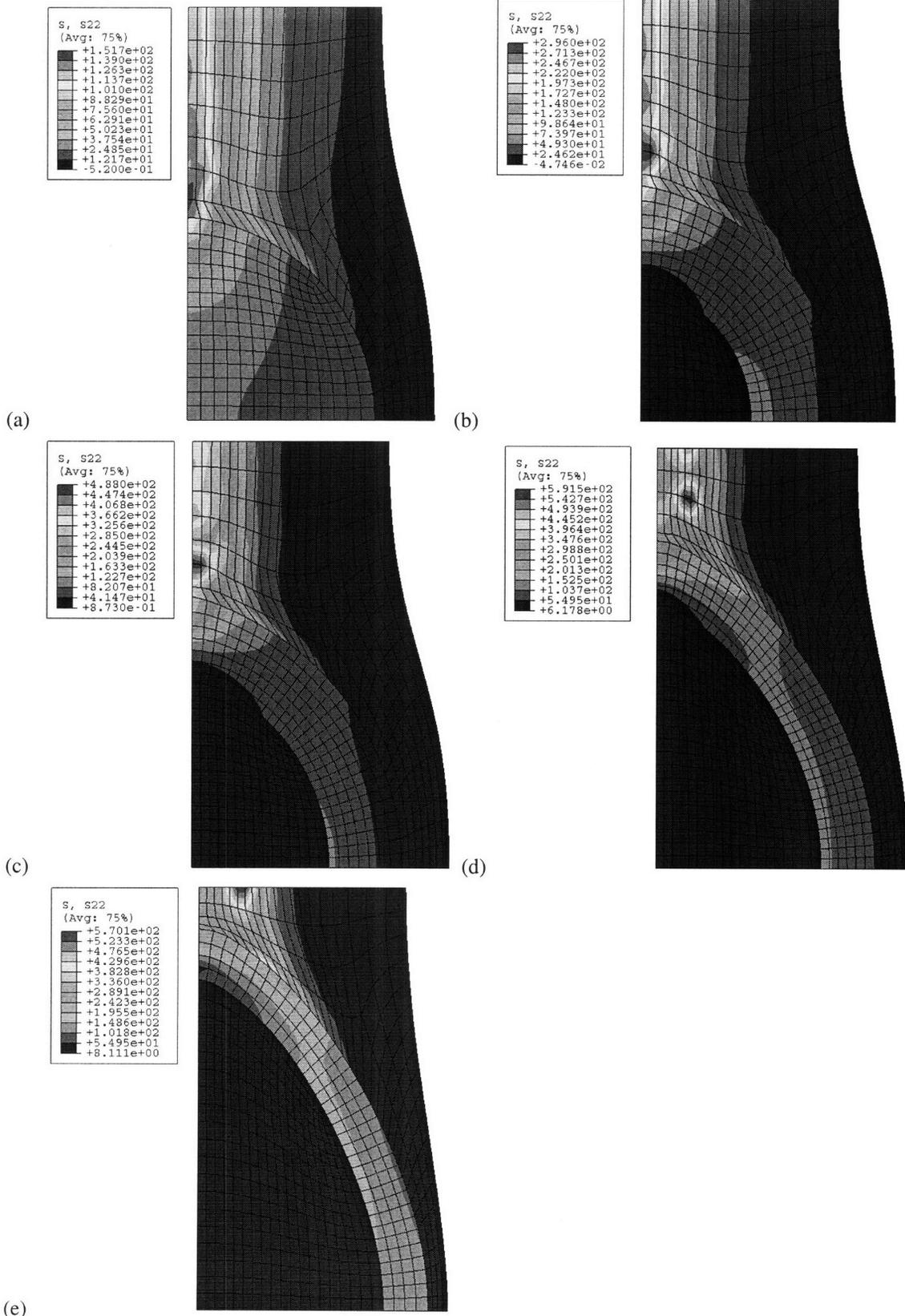


Figure 3.30 shows the stress in the 22 direction at a strain of .5 with a 23% volume fraction of filler particle for varying levels of occluded volume: (a) 0%, (b) 5%, (c) 10%, (d) 20%, (e) 30%.

Increasing the occluded volume increases the stiffness of the material, since the occluded volume effectively increases the amount of filler particle in the matrix. As expected, neither the filler material nor the occluded matrix material takes much of the strain; it is concentrated along the axis above the inclusion.

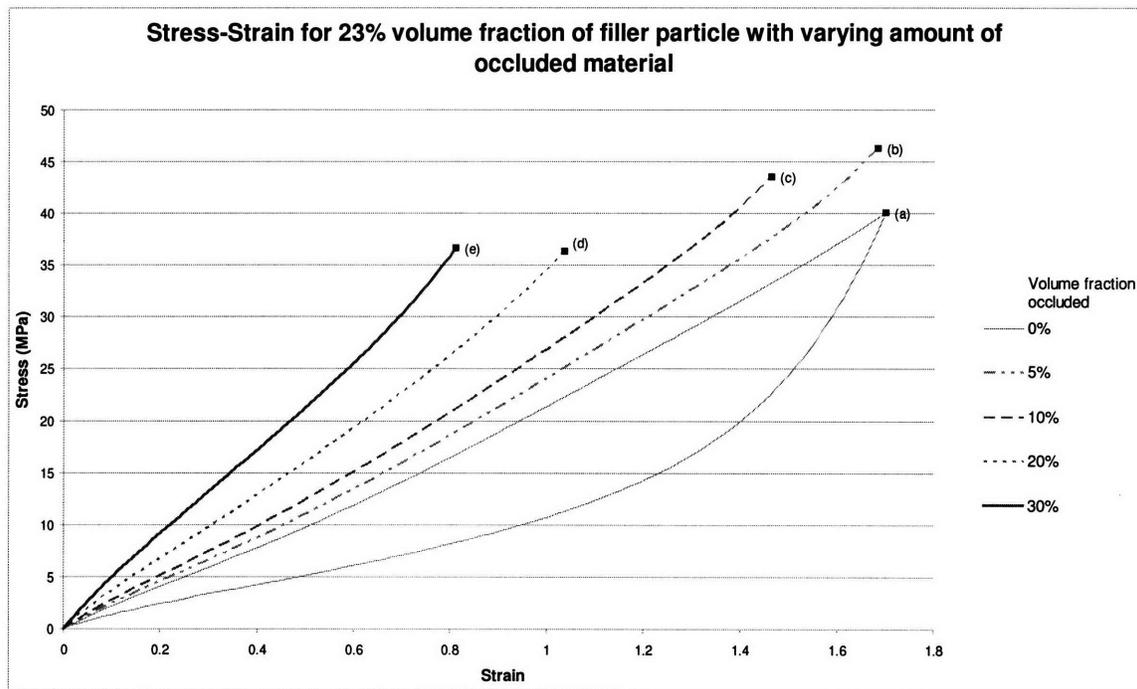


Figure 3.31 shows the stress-strain curves for several different volume fractions of occluded rubber. As the percentage of occluded material increases, so does the stiffness.

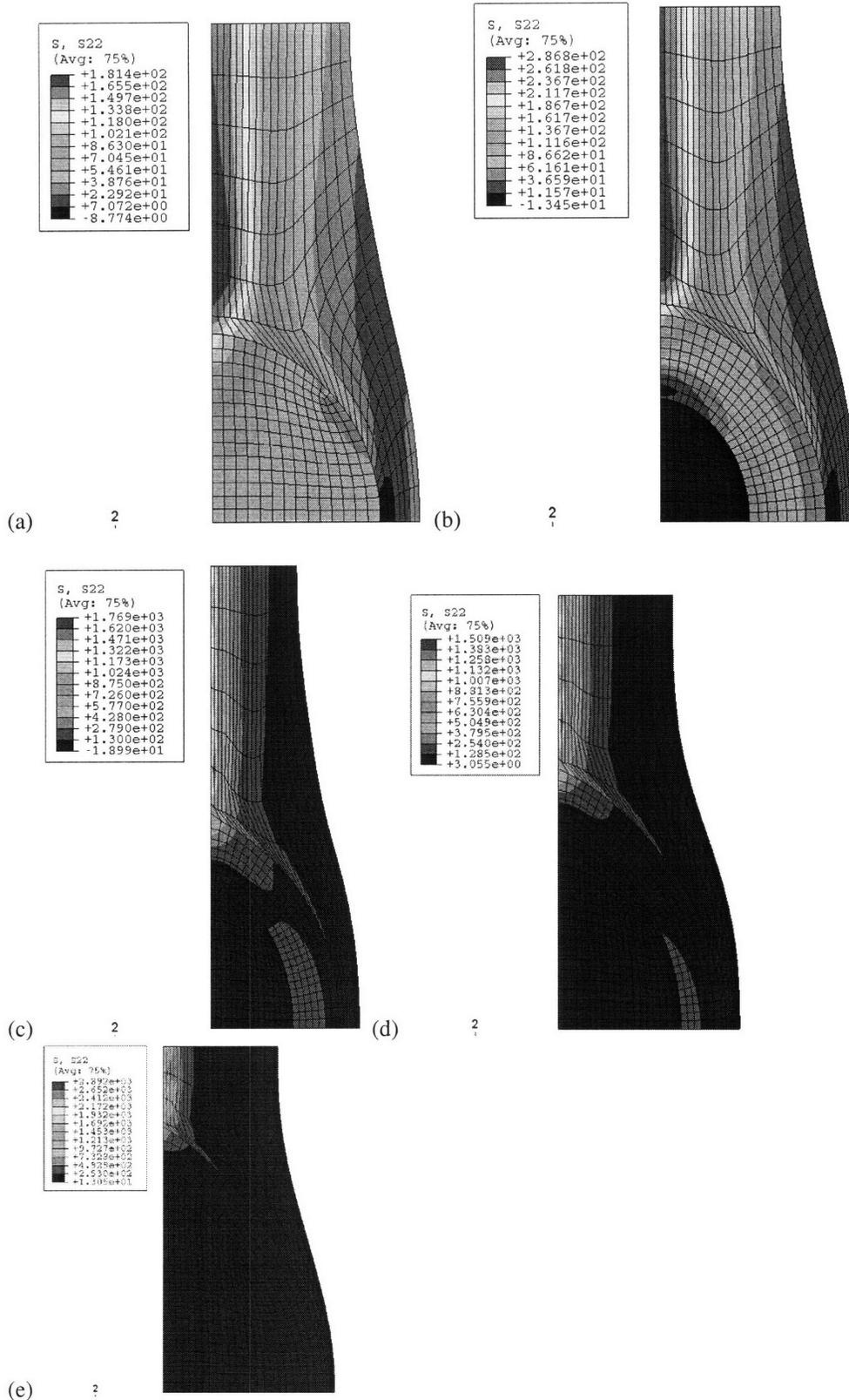


Figure 3.32 shows the stress in the σ_{22} direction for a 23% volume fraction element with varying amounts of occluded rubber at the points indicated on the graph: (a) has 0% occluded, (b) has 5% occluded, (c) has 10% occluded, (d) has 20% occluded, and (e) has 30% occluded.

As seen before in the case with no occluding, the case with softening is less stiff than when there is no softening.

It appears that when approximately 30% of the matrix material is occluded, the stress-strain and stiffness enhancement for a 23% volume fraction of filler are similar to the Harwood and Payne data. The occluded material has a large effect on material behavior, for strains as low as .5, the size of the hysteresis loop increases with the amount of material occluded, and for a material with 30% of the matrix material occluded, the stress level is over twice that of a material with the same amount of filler but no occluded material, as seen in Figure 3.33. The amount of occluded material also affects the evolution of v_s ; as the volume fraction of occluded material increases, the average value of v_s also increases, as seen in Figure 3.34. The necklace structure of filler particles can have a dramatic effect on softening behavior, as the material inside the inclusion does not soften, as seen in Figure 3.35.

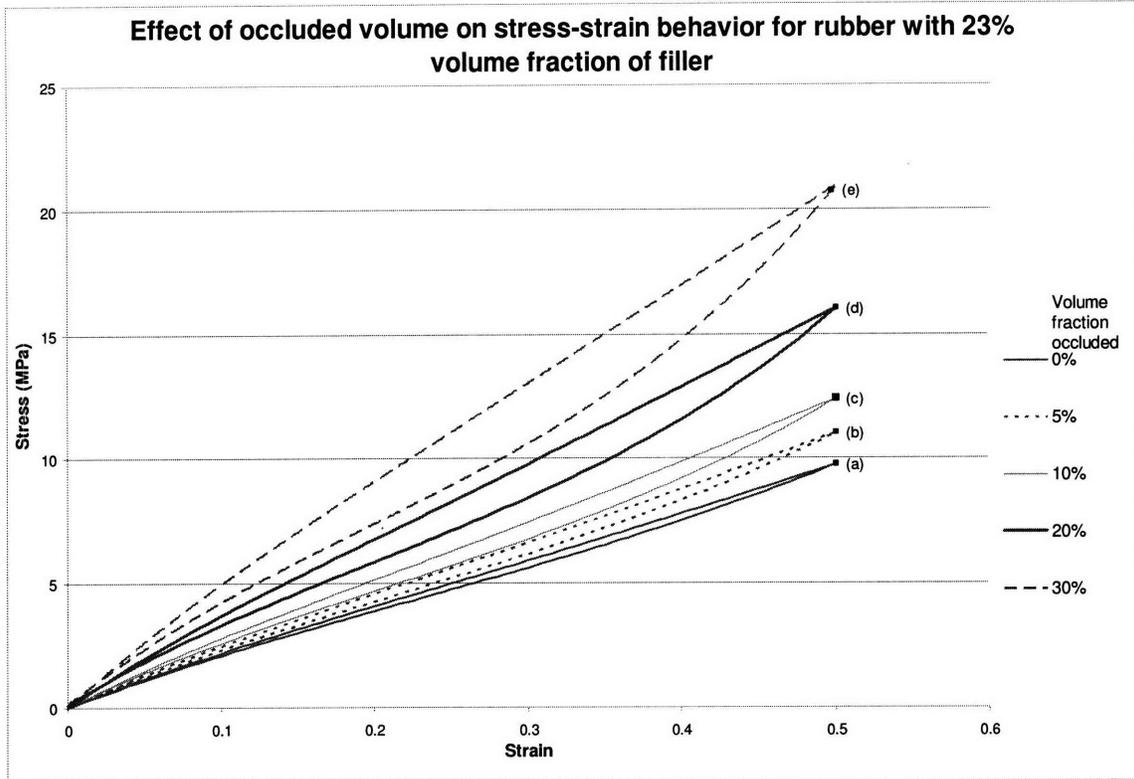


Figure 3.33 shows the stress-strain behavior of rubber with 23% volume fraction of filler particles when loaded to a strain of .5 for varying amounts of occluded rubber.

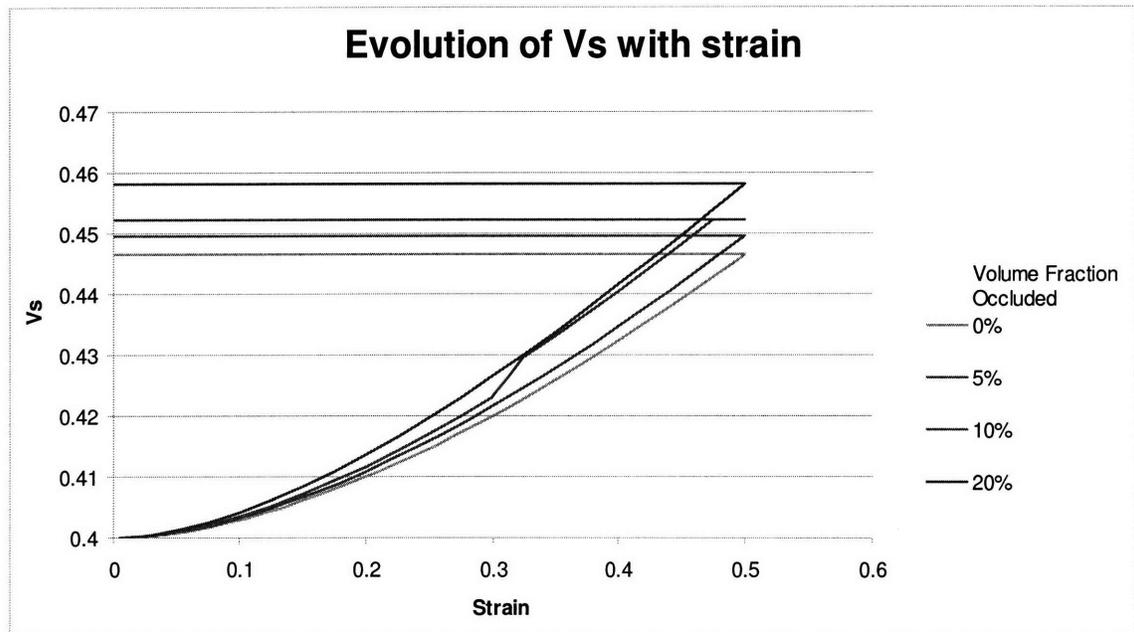


Figure 3.34 shows the evolution of the soft volume fraction of rubber with 23% volume fraction of filler particles when loaded to a strain of .5 for varying amounts of occluded rubber.

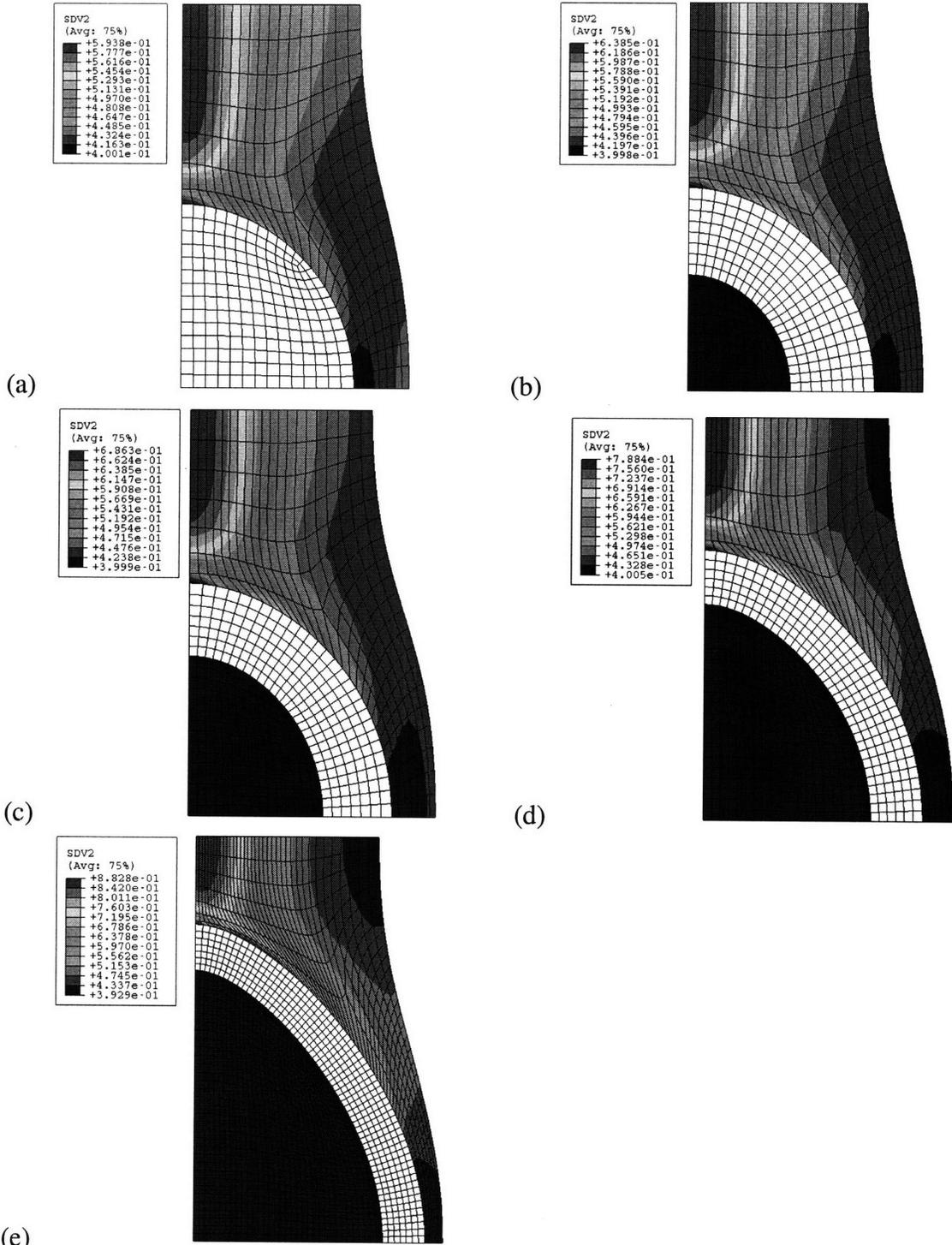


Figure 3.35 shows the evolution in v_s after a strain of .5 for a 23% volume fraction element with varying amounts of occluded rubber: (a) has 0% occluded, (b) has 5% occluded, (c) has 10% occluded, (d) has 20% occluded, and (e) has 30% occluded.

4 Conclusion

The inclusion of filler particles has a significant effect on the behavior of elastomeric materials, increasing stiffness and altering the evolution of the soft domain within the matrix. In unfilled elastomers, softening occurs uniformly, while in filled elastomers, the fraction of soft domain varies, with the greatest amount of soft domain concentrated on the axis in the direction of stretch.

The effects of occluded matrix material are also important, as the amount of material occluded effectively increases the amount of filler particle in the matrix, particularly since the occluded material does not soften.

The data suggests that the evolution of soft volume fraction may account for the greater softening seen in filled elastomers. To further determine whether this is the case, a study could be done looking at the effects of particle/matrix debonding on softening behavior.

References

- [1] Arruda, E.M., Boyce, M.C., "A Three-Dimensional Constitutive Model For the Large Stretch Behavior of Rubber Elastic Materials," *Journal of the Mechanics and Physics of Solids*, Vol. 41. No.2.,1993.
- [2] Arruda, E.M., Boyce, M.C. "Mechanics of Elastomeric Materials," monograph in preparation.
- [3] Bergstrom, J.S., Boyce, M.C., "Mechanical Behavior of Particle Filled Elastomers," *Rubber Chemistry and Technology*, Vol.72, 1999.
- [4] Blanchard, A.F., Parkinson, D., "Breakage of carbon-rubber networks by applied stress," *Ind. Eng. Chem.*, 44, pp799, 1952.
- [5] Boyce, M.C., Socrate, S., "Micromechanics of Toughened Polycarbonate," *Journal of the Mechanics and Physics of Solids*, Vol.48, 2000.
- [6] Bueche, F., "Mullins effect and rubber-filler interaction," *Journal of Applied Polymer Science* 5, 271-281, 1961.
- [7] Dannenberg, E.M., "The effects of surface chemical interactions on the properties of filler-reinforced rubbers," *Rubber Chem. Tech.* 48, 410-444, 1974.
- [8] Harwood, J.A.C. and Payne, A.R., 1966. Stress softening in natural rubber vulcanizates, Part III. *J. Appl. Polym. Sci.* **10**, pp. 315–324.
- [9] Mullins, L., Tobin, N.R., "Stress softening in natural rubber vulcanizates, Part I," *Journal of Applied Polymer Science*, 9, 2993-3010, 1965.
- [10] Rigbi, Z., "Reinforcement of rubber by carbon black," *Advanced Polymer Science*, 36, 21-68, 1980.
- [11] Qi, H.J., Boyce, M.C., "Constitutive Model for Stretch-induced Softening of the Stress-stretch Behavior of Elastomeric Materials," *Journal of the Mechanics of Physics of Solids*, Vol.52, 2004.